Published for SISSA by Springer

Received: *December 30, 2025*
Accepted: *May 21, 2026*
Published: *July 13, 2026*

Search for exotic Higgs boson decays H $\to \mathcal{A}\mathcal{A}$ with $\mathcal{A} \to \gamma\gamma$ in events with a semi-merged topology in proton-proton collisions at $\sqrt{s} = 13$ TeV

The CMS collaboration

Full author list at the end of the paper

E-mail: cms-publication-committee-chair@cern.ch

Abstract: A search for exotic Higgs boson decays $\mathrm{H} \to \mathcal{A}\mathcal{A}$, with $\mathcal{A} \to \gamma\gamma$ is presented, using events with a semi-merged topology. One of the hypothetical particles, $\mathcal{A}$, is assumed to decay promptly into a semi-merged diphoton system reconstructed as a single photon-like object, while the other $\mathcal{A}$ decays into two resolved photons. The search is performed using proton-proton collision data collected by the CMS experiment at $\sqrt{s} = 13\,\text{TeV}$, corresponding to an integrated luminosity of $138\,\text{fb}^{-1}$. The data agree with the standard model background expectation. Upper limits are set on the product of the Higgs boson production cross section and the branching fraction, $\sigma(\mathrm{pp} \to \mathrm{H})\,\mathcal{B}(\mathrm{H} \to \mathcal{A}\mathcal{A} \to 4\gamma)$, which range from 0.264 to 0.005 pb at 95% confidence level, for $\mathcal{A}$ masses in the range $1 < m_{\mathcal{A}} < 15\,\text{GeV}$. These limits are the most stringent to date in the 1–5 GeV $m_{\mathcal{A}}$ range.

Keywords: Beyond Standard Model, Hadron-Hadron Scattering, Higgs Physics, Photon Production

ArXiv ePrint: 2601.00183

https://doi.org/10.1007/JHEP07(2026)119

JHEP07(2026)119

Contents

1 Introduction

The standard model (SM) of particle physics continues to show excellent agreement with measurements performed at the CERN LHC [1] and elsewhere. The search for physics beyond the SM (BSM) has led researchers to look beyond simple decay topologies and towards more exotic signatures. Since the discovery of the Higgs boson (H) by the ATLAS and CMS Collaborations [2–4] in 2012, the Higgs sector has remained a key area for BSM searches. The latest CMS combination of Higgs boson measurements, which uses data from 2015–2018, limits the Higgs boson invisible (undetected) decay branching fraction to less than 13 (25)% at 95% confidence level (CL) [5], leaving open the possibility of additional exotic Higgs boson decays. The Higgs sector is particularly well suited to probe BSM scenarios, as it may provide direct access to BSM states that do not participate in SM gauge interactions. The simplest extensions of the Higgs sector include exotic decays of the form $\mathrm{H} \to \mathcal{A}\mathcal{A}$, where $\mathcal{A}$ is a hypothetical new spin-0 particle decaying to a pair of SM particles [6]. Such decays are found in BSM models containing an additional SM-neutral singlet [6, 7], such as the two-Higgs-doublet model plus singlet (2HDM+S), and are of interest in searches for axion-like particle production [8–11].

Searches for exotic Higgs boson decays of the type $\mathrm{H} \to \mathcal{A}\mathcal{A}$ have been performed at the LHC in several final states. For $\mathcal{A}$ masses above the heavy-fermion thresholds $2m_\tau$ or $2m_\mathrm{b}$, the $\mathcal{A} \to \tau^+\tau^-$ or $\mathcal{A} \to \mathrm{b\bar{b}}$ channels, respectively, are expected to become dominant, as predicted in certain 2HDM+S extensions [12–16]. Below these thresholds, the leptonic mode $\mathcal{A} \to \mu^+\mu^-$ becomes accessible and provides a clean experimental signature [17]. In contrast, the decay $\mathcal{A} \to \gamma\gamma$, although loop-induced and generally subdominant, can become significant in photophilic scenarios where the $\mathcal{A}$ couples to new uncolored charged particles, motivating searches for $\mathrm{H} \to \mathcal{A}\mathcal{A} \to 4\gamma$ [6].

In such scenarios, reconstructing the diphoton invariant-mass spectrum becomes challenging for $\mathcal{A}$ particles with masses of a few GeV produced in $\mathrm{H} \to \mathcal{A}\mathcal{A}$ decays. In the $\mathcal{A}$ mass range of $m_\mathcal{A} \lesssim 1\,\mathrm{GeV}$, $\mathcal{A}$ has a large Lorentz boost, causing the two photons from the $\mathcal{A} \to \gamma\gamma$ decay to be highly collimated. The separation between them becomes equal to or less than the Molière radius ($r_\mathrm{M} = 2.2\,\mathrm{cm}$) of the material of the CMS crystal electromagnetic calorimeter (ECAL), which, in the barrel region, is comparable to the transverse crystal size. The two photons are predominantly reconstructed as a single photon-like object by the standard CMS photon reconstruction algorithms [18], as described in ref. [19]. For $m_\mathcal{A} \gtrsim 1\,\mathrm{GeV}$, the separation between the two photons becomes more distinct. For example, for $1 < m_\mathcal{A} < 2\,\mathrm{GeV}$, the two photons start to become distinguishable, with separations of around 3–5 r_M at the ECAL surface. For $m_\mathcal{A} \gtrsim 10\,\mathrm{GeV}$, the photons are well isolated and fully resolved, allowing the diphoton invariant mass to be reconstructed from the kinematics of both photon objects.

The CMS Collaboration reported on a search [20] for $\mathrm{H} \to \mathcal{A}\mathcal{A} \to 4\gamma$ with four well-isolated photons in the final state, with both photon pairs being fully reconstructed, enabling a search in the $m_\mathcal{A}$ range of 15–62 GeV. The CMS Collaboration also performed a search in the highly boosted regime, where each pair of photons is reconstructed as one merged photon-like object, for $\mathcal{A}$ masses in the 0.1–1.2 GeV range [21]. This direct search, the first of its kind in CMS, can directly measure the invariant mass of the merged diphoton candidates using a novel particle reconstruction technique that employs deep learning algorithms trained on the energy deposits in the ECAL [19]. The ATLAS Collaboration has also reported on an inclusive search for $\mathrm{H} \to \mathcal{A}\mathcal{A} \to 4\gamma$ decays over the full $m_\mathcal{A}$ range of 0.1–62 GeV [22].

The analysis presented in this paper focuses on events with three photon-like objects in the final state, to bridge the gap in the $1 < m_\mathcal{A} < 15\,\mathrm{GeV}$ mass range between the two previous CMS searches mentioned above. The $\mathcal{A}$ particle is assumed to decay promptly into two photons. In this so-called “semi-merged” mass regime, one of the $\mathcal{A} \to \gamma\gamma$ decays produces two well-separated and fully reconstructed photon objects, while the pair of photons from the other $\mathcal{A}$ boson decay is reconstructed as a single photon object. This could occur either because of the actual merging of the photons, or detector and/or reconstruction energy thresholds. The merging of the photons is more common at lower masses, where the opening angle between the two photons is small, and their showers overlap within the ECAL. At higher $m_\mathcal{A}$ values, the photons are more separated, but the secondary photon is often too low in energy to be reconstructed because of the transverse momentum $p_\mathrm{T} > 10\,\mathrm{GeV}$ threshold applied in the standard photon reconstruction [23]. A direct measurement of the invariant mass spectrum in this region by use of traditional methods is thus not possible. Therefore, a novel end-to-end deep learning technique, called the "mass regression", was developed to directly reconstruct $m_{\mathcal{A}}$ from the pattern of energy deposits in the ECAL crystals.

The paper is organized as follows. Section 2 provides a brief overview of the CMS detector. Section 3 outlines the data and simulated samples used in the analysis. The event selection and object identification criteria are detailed in section 4. The mass regression technique based on a deep learning approach is presented in section 5. The signal and background modeling are discussed in section 6. Section 7 summarizes the sources of systematic uncertainty. Finally, section 8 presents the results and their statistical interpretation, and section 9 provides a brief summary. Tabulated results are provided in the HEPData record for this analysis [24].

2 The CMS detector

The CMS apparatus [25, 26] is a multipurpose, nearly hermetic detector, designed to trigger on [27–29] and identify electrons, muons, photons, and (charged and neutral) hadrons [23, 30, 31]. The central feature of the CMS apparatus is a superconducting solenoid of 6 m internal diameter, providing a magnetic field of 3.8 T. Within the solenoid volume are a silicon pixel and strip tracker, a lead tungstate crystal ECAL, and a brass and scintillator hadron calorimeter (HCAL), each composed of a barrel and two endcap sections. Forward calorimeters extend the pseudorapidity (η) coverage provided by the barrel and endcap detectors. Muons are detected in gas-ionization chambers embedded in the steel flux-return yoke outside the solenoid. A global "particle-flow" (PF) algorithm [18] aims to reconstruct all individual particles in an event by combining information from the all-silicon inner tracker, the ECAL and HCAL, and the muon system. The reconstructed particles are used to build τ leptons, jets, and missing transverse momentum [32–34]. Events of interest are selected using a two-tiered trigger system. The first level, composed of custom hardware processors, uses information from the calorimeters and muon detectors to select events at a rate of around 100 kHz within a fixed latency of 4 μs [27]. The second level, known as the high-level trigger, consists of a farm of processors running a version of the full event reconstruction software optimized for fast processing, and reduces the event rate to a few kHz before data storage [28, 29].

The ECAL consists of 75 848 lead tungstate crystals, which provide a coverage of $|\eta| < 1.48$ in the barrel region (EB) and $1.48 < |\eta| < 3.00$ in the two endcap regions. The full azimuthal range $|\phi| < \pi$ is covered for all regions. In the EB, which is the focus of this paper, an energy resolution of about 1% is achieved for photons in the tens of GeV energy range, for those that do not convert to an e^+e^- pair before reaching the EB. The energy resolution for photon conversions in the EB is about 1.6% up to $|\eta| = 1$, rising to about 3% at $|\eta| = 1.48$ [26]. Each EB crystal has dimensions of $2.18 \times 2.18 \times 23$ cm^3. This corresponds to a transverse granularity of $\Delta\eta \times \Delta\varphi = 0.0174 \times 0.0174$ for electromagnetic showers from particles originating in the center of the CMS detector. Since the crystal Molière radius is comparable to the crystal width, more than 90% of the energy of photons interacting only in the ECAL is laterally contained within a 3×3 crystal matrix [23].

The material structure of the inner tracking detectors changes with pseudorapidity. As a result, the number of radiation lengths (X_0) that a photon traverses before reaching the EB surface varies from $0.4\,X_0$ along the central plane ($\eta \approx 0$) up to $1.8\,X_0$ on the forward edge

($\eta \approx 1.4$). Correspondingly, the amount of energy that a photon loses, and its probability to convert into an e^+e^- pair before reaching the ECAL crystals varies with η.

Finally, an important feature of the proton collisions at the LHC is the presence of additional, soft collisions concurrent with the primary hard-scattering event. Such additional proton-proton (pp) interactions within the same or nearby bunch crossings, known as pileup, can contribute additional energy depositions, particularly in the ECAL. Since these energy deposits may potentially be misidentified as photons, appropriate pileup mitigation techniques are applied [35]. A more detailed description of the CMS detector, together with a definition of the coordinate system used and the relevant kinematic variables, is reported in refs. [25, 26].

3 Data samples and simulated events

The analysis is performed using pp collision data at $\sqrt{s} = 13\,\text{TeV}$, collected with the CMS detector at the LHC from 2016 to 2018, corresponding to an integrated luminosity of $138\,\text{fb}^{-1}$. Simulated $\text{H} \to \mathcal{A}\mathcal{A} \to 4\gamma$ samples generated with $m_{\mathcal{A}} = 1$, 3, 5, 10, and 15 GeV are used to define the signal model, as discussed in section 6. These values are chosen to evenly cover the signal mass phase space targeted in this analysis. They are generated with MadGraph5_aMC@NLO (v2.5.5) [36] at leading-order (LO) using the SM + Dark Vector + Dark Higgs boson model [6, 7] and a Higgs boson mass of 125 GeV with its SM width, with up to one associated jet and negligible lifetime of $\mathcal{A}$. While the underlying model can accommodate different lifetimes of $\mathcal{A}$ depending on the couplings, only the prompt scenario is considered in this analysis. The parton distribution functions provided by NNPDF3.1 [37] at next-to-next-to-leading order accuracy are used. The generated hard process is interfaced with PYTHIA (v8.240) [38] to simulate hadronization and the pp underlying event, following the CP5 [39] tune. The generated samples are processed through the CMS detector simulation based on Geant4 [40], using the same reconstruction algorithms used on data. The dominant backgrounds in this search are SM events composed uniquely of jets produced through the strong interaction, referred to as quantum chromodynamics (QCD) multijet events, as well as $\gamma + \text{jet}$ and prompt diphoton production. The background contributions are modeled entirely from data in this analysis, and no simulated events are used to describe them.

Additional simulated minimum bias interactions are overlaid on all simulated events to account for pileup effects. Along with the simulated samples, interpolated signal shapes are also used to ensure comprehensive coverage.

4 Event selection and reconstruction

The events in the data are required to pass the diphoton high-level trigger selection used in the CMS low-mass $\text{H} \to \gamma\gamma$ search [41], which requires the triggered diphoton objects to have an invariant mass greater than 55 GeV, with the photon minimum p_{T} thresholds of 30 and 18 GeV on the highest and second-highest p_{T} photons, respectively, as well as various calorimeter-based identification criteria. Photon reconstruction [23] in CMS starts by clustering ECAL crystal energy deposits. For photons with transverse energy greater than 10 GeV, clusters are grouped into superclusters to account for shower spread from tracker interactions and the magnetic field. Below this threshold, or if quality criteria fail, individual clusters may still be reconstructed as photon-like PF [18, 42] candidates. Events that pass the trigger are required to pass the photon reconstruction and kinematic selection requirements similar to those used in the CMS SM $\mathrm{H} \to \gamma\gamma$ search [43]. Each photon candidate is required to satisfy standard CMS identification criteria that ensure the electromagnetic shower is compact, well-contained in the ECAL, and largely unaccompanied by hadronic energy or nearby tracks. These selections are designed to identify prompt, isolated photons and to suppress contamination from jets and electrons. The leading and subleading photons must have $p_{\mathrm{T}} > 30$ and $18\,\mathrm{GeV}$, respectively, and satisfy loose isolation and electron veto requirements [44].

To account for the distinct kinematic and topological features of the $\mathcal{A} \to \gamma\gamma$ decay, the photon identification is further refined, following the same strategy as the CMS fully merged diphoton analysis [21], as described below. Discrimination between signal photons and background jets is achieved by using the photon vs. electromagnetic (EM) -enriched jet multivariate discriminator [43]. Here, EM-enriched jets refers to hadronic jets with a large EM energy fraction, typically originating from neutral meson decays such as $\pi^0, \eta \to \gamma\gamma$. As the opening angle between photons from $\mathcal{A} \to \gamma\gamma$ increases with $m_{\mathcal{A}}$, their showers become more similar to those produced by EM-enriched jets. To maintain high signal efficiency in this regime, a looser requirement is applied to the discriminator output than in the CMS $\mathrm{H} \to \gamma\gamma$ search. This relaxation naturally increases the rate of hadronic jet contamination, which is mitigated by applying a more restrictive requirement on the charged-hadron isolation, I_{ch}, defined as the transverse momentum of charged particles in a cone around the selected photon. Selected events are required to contain exactly three reconstructed photons (Γ) that pass the above photon identification criteria, and have the invariant mass of the triphoton system within the range $90 < m_{\Gamma\Gamma\Gamma} < 180\,\mathrm{GeV}$, which contains the Higgs boson signal mass window and sidebands. This analysis only uses photons in the EB ($|\eta| < 1.44$). This requirement retains approximately 80–90% of the signal for $m_{\mathcal{A}}$ ranging from 1 to $15\,\mathrm{GeV}$, indicating that the majority of signal photons are found in the barrel. The use of the endcaps would require the development of a special strategy for the merged candidate mass regression in a complicated geometric environment. Studies allowing resolved photons in the endcaps, while requiring the merged candidate to be in the EB, show only a percent-level increase in the signal efficiency across the mass range considered. Therefore, the EB-only selection is adopted to maintain a uniform reconstruction strategy. After applying all of the selection criteria to the simulated samples, signal events are selected with an estimated efficiency of 2.8–5.6%. The overall signal efficiency is mainly limited by the trigger requirements and by the requirement of exactly three reconstructed photons in the event, which defines the semi-merged topology targeted in this analysis. At small $m_{\mathcal{A}}$, where the fully merged topology becomes more prevalent, this requirement leads to a larger reduction in acceptance. Further reduction in efficiency arises from the photon identification and isolation requirements that affect all signal masses.

The three reconstructed photons that pass the preselections are grouped into two classes of $\mathcal{A}$-particle candidates: merged ($\mathcal{A}1$) and resolved ($\mathcal{A}2$) candidates. The resolved candidates $\mathcal{A}2$ are reconstructed by choosing the two closest photons and using their momenta to obtain the invariant mass. From simulation, this is seen to correctly match the photons from the same parent $\mathcal{A}$ particle 97–99% of the time for various $m_{\mathcal{A}}$. The merged candidate $\mathcal{A}1$ in

JHEP07(2026)119

semi-merged events is obtained from the third reconstructed photon, for which a direct measurement of the invariant mass is not possible with the reconstructed objects, and so the mass is reconstructed from the machine learning (ML) based regression.

Each reconstructed $\mathcal{A}$-particle candidate is used to fill a two-dimensional (2D) $m_{\mathcal{A}}$ shape template, which acts as either a signal or background model. Under the identical mass hypothesis, $m_{\mathcal{A}1} = m_{\mathcal{A}2}$, the nominal signal would fall on the diagonal of this 2D plane. In addition, we also define an orthogonal signal region (SR) within the Higgs boson mass window on the triphoton mass $m_{\Gamma\Gamma\Gamma}$, under the assumption that the photon-like objects come directly from Higgs boson decays, with no additional invisible particles. The SR and sideband (SB) regions along the $m_{\Gamma\Gamma\Gamma}$ axis are:

- m_{H}-SB$_{\mathrm{low}}$: $90 < m_{\Gamma\Gamma\Gamma} < 100\,\mathrm{GeV}$,
- m_{H}-SR: $100 < m_{\Gamma\Gamma\Gamma} < 135\,\mathrm{GeV}$,
- m_{H}-SB$_{\mathrm{high}}$: $135 < m_{\Gamma\Gamma\Gamma} < 180\,\mathrm{GeV}$,

while the SR and SB along the 2D $m_{\mathcal{A}}$ axis are:

- $m_{\mathcal{A}}$-SB: $\Delta m_{\mathcal{A}} > 2\,\mathrm{GeV}$ (off-diagonal),
- $m_{\mathcal{A}}$-SR: $\Delta m_{\mathcal{A}} < 2\,\mathrm{GeV}$ (on-diagonal).

The boundaries of the regions above are optimized using simulation to maximize the signal efficiency in the SR and minimize the signal contamination in the SBs, while maintaining a sufficient number of events in the SBs to have a reasonable background estimate. The shape and yield of the nonresonant background in the final SR are derived using the data sidebands in the $m_{\Gamma\Gamma\Gamma}$ and 2D $m_{\mathcal{A}}$ regions described above.

5 Signal mass regression using a graph neural network

Several LHC studies have explored the ML-based reconstruction of Lorentz-boosted particle decays [45–47], most often relying on PF candidates. While these studies show improved results over the traditional cutoff-based algorithms, their effectiveness in dealing with shower merging remains limited. This motivates an end-to-end strategy that minimizes intermediate preprocessing, enabling ML models to train directly on minimally processed detector data represented as detector images or permutation-invariant graphs, to predict the particle properties [48–52]. In CMS, data are organized into various tiers according to the level of processing [53, 54]. While compact, clustered formats are optimized for most analyses, studies like this one require access to detailed calorimeter information available only in minimally processed data, which enables the reconstruction of merged-photon candidates using the mass regression described below.

In the semi-merged regime of the $\mathrm{H} \to \mathcal{A}\mathcal{A} \to 4\gamma$ decay explored in this search, one pair of photons from the $\mathcal{A}$ decay is resolved and reconstructed as two separate photons. At the same time, the other pair could be highly collimated and reconstructed as a single photon, or the secondary photon in this pair, while identifiable as a separate object, could remain unreconstructed. This can happen if the secondary photon is well separated from the primary photon, but is too low in energy ($p_T < 10$ GeV) to be reconstructed by the standard CMS PF algorithm, or the opening angle is large so that the secondary photon escapes into the endcap or falls out of the search window. In simulation, we find that at $m_{\mathcal{A}} = 1$ GeV, the merged leg is dominated by true overlaps of the two photon showers, comprising more than 90% of events. For larger masses, the semi-merged configuration with a soft secondary photon is the dominant contribution, accounting for roughly 75–95 (65–85)% of events for $m_{\mathcal{A}}$ values in the range 3–5 (10–15) GeV, corresponding to cases where the secondary photon is contained within the regression window. To handle these cases, the mass regression mentioned above is used to determine the underlying $\mathcal{A}$ mass directly from the crystal-level patterns in the ECAL, an approach similar to that developed in ref. [19] and used in ref. [21]. For larger $m_{\mathcal{A}}$, a larger fraction of events have a secondary photon that falls outside the regression window, resulting in a single-photon-like topology and reduced signal efficiency in the final SR.

While the approach described in ref. [19] employs a convolutional neural network (CNN), this analysis uses a more advanced graph neural network (GNN), which has been found to outperform the CNN. The choice of a GNN was motivated by several factors. Graph convolution operations can naturally learn rotational symmetries present in the energy deposit patterns in the calorimeter in the presence of soft secondary photon deposits by utilizing permutation invariance, which is a challenge for CNNs, thus removing one level of complexity from the problem. The use of a graph format for the input data also enables the use of only those crystals that have energy deposited in them. This results in a substantial reduction of the problem size relative to CNNs, where the data are represented by large, very sparse, 2D grids.

5.1 Model architecture and input images

The mass regression is built with a GNN, called a dynamic reduction network [55], with residual connections added. The inputs to the nodes of the graph are the energy deposit maps from the EB. A 128×128 matrix of ECAL crystals around the most energetic crystal (seed) of the reconstructed merged photon candidate is chosen to create an image array. This corresponds to a window within an angular distance $\Delta R = \sqrt{\Delta\eta^2 + \Delta\phi^2} \approx 1.11$ around the seed. Given that the opening angle between the photons from the $\mathcal{A}$ increases with its mass $m_{\mathcal{A}}$, the width of this window is chosen such that it captures most of the secondary photon's energy deposits. More than 90% of events fall inside the window for $m_{\mathcal{A}} < 5$ GeV, and about 60–80% for higher masses up to 15 GeV.

Examples of the ECAL energy deposit maps fed into the network are shown in figure 1, taken from $\mathrm{H} \to \mathcal{A}\mathcal{A} \to 4\gamma$ simulation samples of different signal masses that correspond to different boosts and opening angles. The maps are plotted in the relative ECAL crystal index coordinates ($i\eta'$, $i\phi'$), corresponding to the crystal positions along the η and ϕ directions inside the cropped window around the merged-photon candidate. Every pixel in the image directly represents the energy deposited in an individual ECAL crystal. These energy deposits correspond to the interaction between the incoming photon and the detector material.

In figure 1, the merged-photon candidate is shown at the center of each image, with the generator-level opening angle between the two photons, $\Delta R_{\text{gen}}(\gamma\gamma)$, printed above in terms of ECAL crystals. For the lowest mass point ($m_{\mathcal{A}} = 3$ GeV, left), a second overlapping energy cluster is visible near the central deposit, consistent with two closely spaced photons being

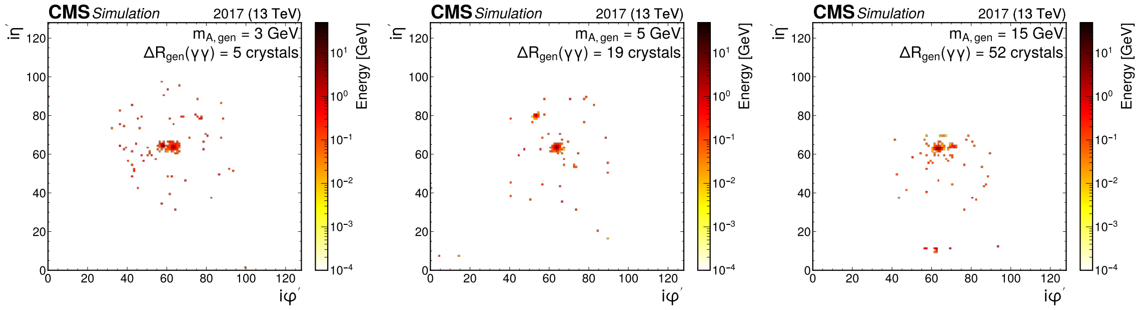

Figure 1. Energy deposit maps in the ECAL from simulated $\mathrm{H} \to \mathcal{A}\mathcal{A} \to 4\gamma$ events corresponding to the 2017 data-taking conditions for the masses $m_{\mathcal{A}} = 3$ (left), 5 (middle), and 15 (right) GeV, shown in the relative ECAL crystal index coordinates ($i\eta'$, $i\phi'$). Each image displays the ECAL deposits from a single $\mathcal{A} \to \gamma\gamma$ decay of the merged leg. A close-up of the merged-photon candidate in the center of each image is shown, and the generator-level photon separation $\Delta R_{\mathrm{gen}}(\gamma\gamma)$ is indicated above each panel for the corresponding mass point.

reconstructed as a single merged photon. At higher masses, the photons are more widely separated (as indicated by the larger opening angles); in the middle image, the secondary photon corresponds to the cluster to the upper left of the central deposit, while in the rightmost image, it corresponds to the low-energy cluster at the bottom. These secondary photon deposits are very low in energy and fall below the reconstruction threshold.

To fully utilize the differences in the EM shower development that result from the differences in the material budget in the η-direction in the detector, the ECAL energy deposit map is split into the transverse and longitudinal energy components, defined as $E_{\mathrm{T}} = E \sin\theta$ and $E_z = E \cos\theta$ respectively, where E is the energy and θ is the polar angle of the energy deposit relative to the beam line. Additionally, the position coordinates of the crystals in x, y, and z are also provided as separate features. These position coordinates, along with the relative location of energy deposits, aid in defining adjacency relations within the network and help the model to learn global variations in shower patterns due to differences in material budget as a function of η.

The architecture of the network is illustrated in figure 2. The input nodes, which encode the information from the energy deposits, are first projected into a high-dimensional space using a multilayer perceptron (MLP) [56], a fully connected neural network. The core of the model consists of edge convolution (EdgeConv) [57] modules. In each module, a graph is dynamically constructed by connecting each node to its nearest 16 neighbors in the learned feature space. The EdgeConv operation is then applied to these edges to update the node features. Following this, the original node features are added to those updated by the EdgeConv, forming a residual connection, before applying pooling. This residual connection, combined with pooling, progressively reduces the graph size. After the final clustering and pooling stage, global max pooling is applied across the remaining nodes, and the resulting feature vector is passed through an output MLP with a single node. This output is compared to the true mass of the object responsible for the input energy pattern using the mean absolute error as the loss function.

JHEP07(2026)119

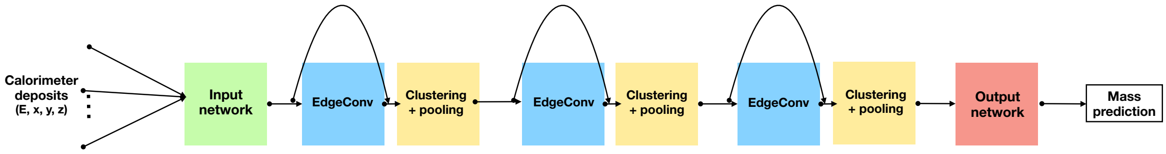

Figure 2. Illustration of the network architecture used for the mass regression. Input energy and position of the calorimeter deposits are processed by an MLP, followed by EdgeConv and clustering + pooling layers with residual connections. The final graph representation is passed through an output MLP to predict the object mass.

5.2 Training

For training, additional sets of simulated samples of $\mathcal{A} \to \gamma\gamma$ decays were produced with flat distributions in $m_{\mathcal{A}}$ and p_{T}, within the ranges $m_{\mathcal{A}} = (0,\ 18)$ GeV and $p_{\mathrm{T}} = (10,\ 200)$ GeV, and restricted to the EB, with $|\eta| < 1.44$. The photon selection criteria defined for merged photon-like candidates preferentially select highly boosted $\mathcal{A}$ particles, which tends to sculpt the $p_{\mathrm{T}}^{\mathcal{A}}$ vs. $m_{\mathcal{A}}$ phase space. To avoid biasing the network, the training samples are produced to ensure that the $(p_{\mathrm{T}}^{\mathcal{A}}, m_{\mathcal{A}})$ phase space is uniformly distributed after photon selection criteria have been applied.

At the boundaries of the training phase space, the performance of any deep neural network tends to degrade because those regions are underrepresented in the training data, leading to reduced generalization and biased predictions. To mitigate this effect and better equip the network to distinguish genuine merged-photon candidates from $\mathcal{A}$ decays from single photons originating from background processes, simulated single-photon samples are also included in the training set. These single photons are assigned a random negative target mass value in the range -3 to 0 GeV, following the "domain continuation" method described in ref. [19]. The minimum value of -3 GeV is optimized from training such that the mass response is linear, and with a minimal contribution of single photons in the mass domain of interest, $m_{\mathcal{A}} > 0$ GeV. By augmenting the training set with true photons not associated with the $\mathcal{A} \to \gamma\gamma$ decays and assigning a nonphysical negative mass value, we effectively reduce the background contamination by removing the samples that become regressed with masses below zero during inference, while making the full low-$m_{\mathcal{A}}$ region accessible to the network.

After the photon selection criteria are applied, the available samples, corresponding to the 2017 data-taking conditions, are split into independent training and validation subsets, with the latter used only to monitor performance during training. In total, about 600k $\mathcal{A} \to \gamma\gamma$ events and 70k single-photon events are used, split in an approximately 4:1 ratio between the training and validation sets. The number of single-photon events is chosen such that the density of negative-mass samples is the same as that of the positive-mass samples. The regressed mass as a function of the true mass is shown in figure 3, demonstrating that the training works as intended: the regression learns the true mass efficiently over the entire mass range.

JHEP07(2026)119

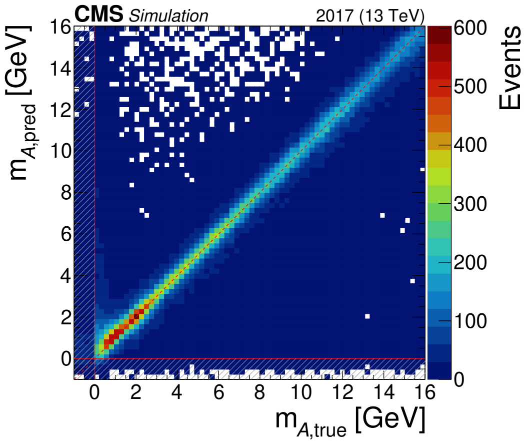

Figure 3. True vs. predicted mass from the mass regression during training validation using simulated $\mathcal{A} \to \gamma\gamma$ samples corresponding to the 2017 data-taking conditions generated with a continuous uniform distribution in mass and p_T. As discussed in section 5.2, the training includes domain continuation, which introduces negative target mass labels to improve linearity near the boundary; regions below and to the left of the solid red lines correspond to these negative mass predictions, which are not considered in the final selection.

5.3 Validation on simulation and data

The regression model is validated on fixed-mass simulated samples of the signal $H \to \mathcal{A}\mathcal{A} \to 4\gamma$, for various $\mathcal{A}$ particle masses. Figure 4 shows the mass regression prediction for the merged photon candidates that pass the selections, for the signal samples of various masses. It can be seen that the regression can reconstruct the mass peaks reasonably well for all $m_{\mathcal{A}}$ points. As the mass increases, there is an increasing peak at $m_{\mathcal{A}} \sim 0$ GeV because the "merged leg" looks more like a single photon, either because the secondary photon is extremely low in energy or the opening angle is too high, so it goes out of the image window. Figure 5, which shows simulated samples corresponding to different data-taking periods, demonstrates that the predicted mass peaks are well aligned for a signal mass of 5 GeV. It highlights the robustness of the regression network to differences in conditions among different data-taking periods, given that it was trained exclusively using simulated samples corresponding to the 2017 data-taking period.

Since the signal models are built from simulated events and compared to background models derived from data, calibration and adjustment of the response of the mass regression between data and simulation are also performed. Although decays of neutral mesons such as η and π^0 might seem suitable for this purpose, the selected events often contain highly collimated QCD jets with multiple mesons, which lead to shifted predicted masses. Additionally, limited simulation statistics and potential mismodeling of QCD processes make reliable comparisons with the data challenging. Another candidate, the J/ψ meson, was considered; however, selecting boosted J/ψ mesons that match the $\mathcal{A}$ particle kinematics yielded an extremely low number of events, rendering it unsuitable for a meaningful calibration.

Instead, we turn to the decays of $Z \to e^+e^-$, following the approach used in the fully merged diphoton search [21]. The electrons from the decay are produced in abundance and are well isolated from hadronic activity, similar to the case of the $\mathcal{A} \to \gamma\gamma$ decays. When

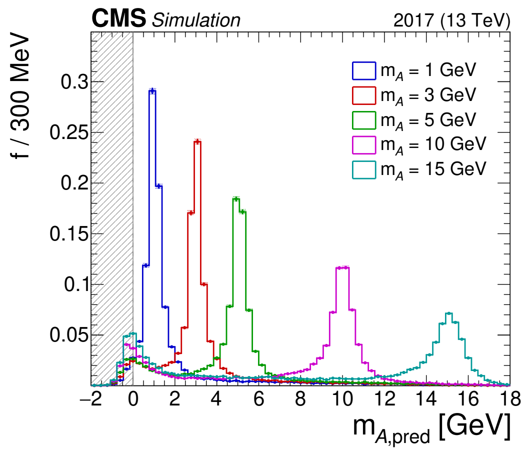

Figure 4. Predicted mass distribution from the mass regression on the merged leg of the simulated $\mathrm{H} \rightarrow \mathcal{AA} \rightarrow 4\gamma$ events corresponding to the 2017 data-taking conditions, which pass the event selection criteria, for different simulated mass points. The variable f denotes the fraction of events per bin. The area of each distribution is normalized to unity. Negative mass predictions shown in the hatched region are not considered for final selections.

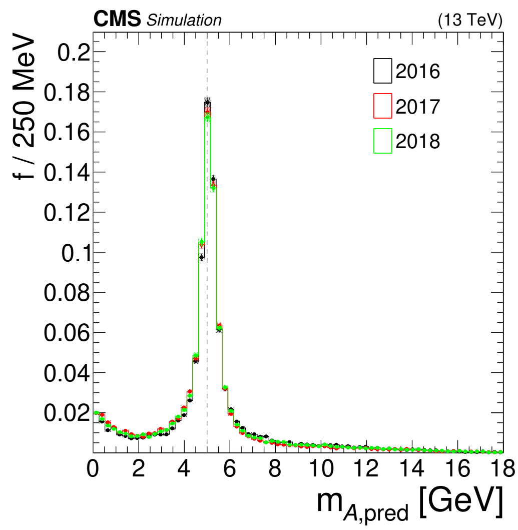

Figure 5. Predicted mass distribution from the mass regression on the merged leg of the simulated $\mathrm{H} \rightarrow \mathcal{AA} \rightarrow 4\gamma$ events with $m_{\mathcal{A}} = 5\,\mathrm{GeV}$, reconstructed under detector conditions corresponding to the 2016, 2017, and 2018 data-taking periods. The same regression and event selection are applied in all cases. The variable f denotes the fraction of events per bin. The area of each distribution is normalized to unity.

JHEP07(2026)119

interacting with the magnetic field of the CMS solenoid, the electron shower gets slightly smeared and can resemble a highly merged photon shower from the $\mathcal{A}$. The regression is validated on the *single* electron showers which peak around $m \approx 0\,\text{GeV}$. Electron candidates are obtained using the "tag-and-probe" method [58] and are required to be matched to a photon candidate passing the photon identification criteria. In addition to this, to better represent semi-merged-like events characterized by a soft secondary energy deposit near the primary photon deposit, we examine a specific subset of the selected events. These contain low-energy photon-like PF candidates mentioned in section 4. The p_T spectrum of these deposits has been verified in simulation to overlap with that of the secondary photon from $\mathcal{A} \to \gamma\gamma$ decays across all signal mass points, confirming the kinematic representativeness of this proxy.

The resulting mass distributions are shown in figure 6: the left panel corresponds to all selected $\mathrm{Z} \to \mathrm{e}^+\mathrm{e}^-$ events, peaking near zero, while the right panel shows the subset with a nearby soft PF deposit, producing a shifted distribution characteristic of semi-merged topologies. The relative response between data and simulation is parameterized using two components: a mass-scale variation, which adjusts the overall scale of the simulated regressed mass, and a smearing variation, which introduces extra Gaussian smearing to match the resolution observed in data. These variations are evaluated separately for each data-taking year and for three EB pseudorapidity regions: central ($|\eta| < 0.5$), middle ($0.5 < |\eta| < 1.0$), and forward ($1.0 < |\eta| < 1.44$). A representative example using 2017 data and simulation over the full EB pseudorapidity range is shown in the figure. The derived variations are incorporated as systematic uncertainties in the signal model, as discussed in section 7. In figure 6, the shaded red band corresponds to the uncertainty envelope from the scale and smearing variations. These are applied as one-sided systematic variations (shift or no shift), and the resulting envelope spans the possible upward or downward shift of the prediction relative to the nominal simulation. The data and simulation show agreement within the assigned uncertainties, with the residual differences at the percent level. This provides a validation of the calibration in configurations relevant for semi-merged topologies as well.

6 Signal and background models

6.1 Signal model

The final SR is defined as $m_\mathrm{H}\text{-SR} \cap m_\mathcal{A}\text{-SR}$. In this region, we construct a signal model that specifies both the shape of the distribution and its total yield (normalization) with respect to the data for a given integrated luminosity, for each $m_\mathcal{A}$ hypothesis. The shape is derived by creating the 2D $m_\mathcal{A}$ template using the simulated $\mathrm{H} \to \mathcal{A}\mathcal{A} \to 4\gamma$ events passing the event selection criteria described in section 4. Simulated samples are generated at nominal $\mathcal{A}$ mass points of $m_\mathcal{A} = 1$, 3, 5, 10, and 15 GeV, for which a shape template is produced and compared against the estimated background model.

The yield or normalization $N(m_\mathcal{A}|m_\mathrm{H}\text{-SR} \cap m_\mathcal{A}\text{-SR})$ in the final SR for a particular $m_\mathcal{A}$ hypothesis with the data corresponding to a given integrated luminosity $\int \mathcal{L}\,\mathrm{d}t$ is given by:

$$N(m_\mathcal{A}|m_\mathrm{H}\text{-SR} \cap m_\mathcal{A}\text{-SR}) = \sigma(\mathrm{pp} \to \mathrm{H})\, \mathcal{B}(\mathrm{H} \to \mathcal{A}\mathcal{A} \to 4\gamma)\, \varepsilon(m_\mathcal{A}|m_\mathrm{H}\text{-SR} \cap m_\mathcal{A}\text{-SR}) \int \mathcal{L}\,\mathrm{d}t, \tag{6.1}$$

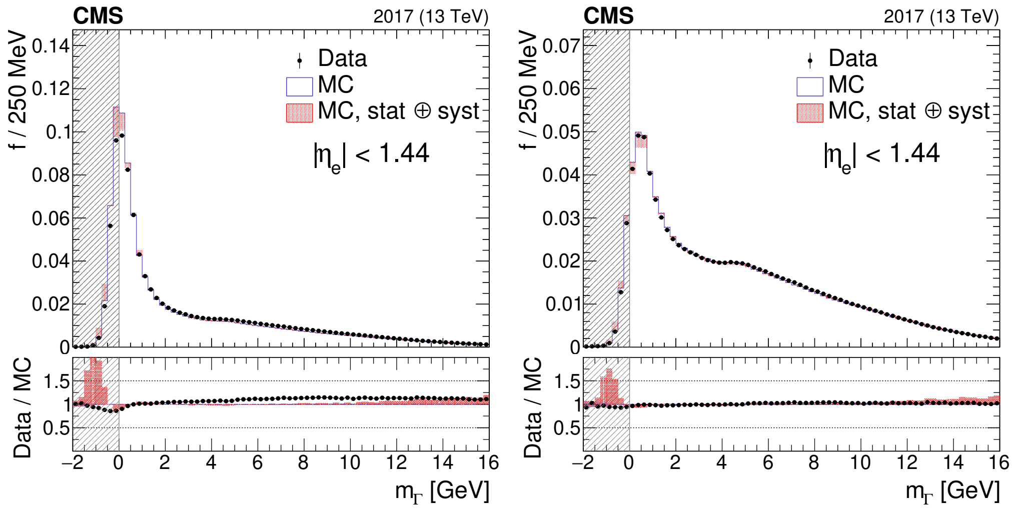

Figure 6. Regressed mass for $Z \to e^+e^-$ electrons in the 2017 data vs. simulation for all events passing the selections (left), showing a peak at zero, and for a subset of those events with a soft photon-like deposit near the electron (right), showing a peak away from zero. The variable f denotes the fraction of events per bin. The area of each distribution is normalized to unity. In the upper panels of each plot, the coverage of the best fit scale and smearing estimates in simulated events ("MC, stat $\oplus$ syst"), plus statistical uncertainties added in quadrature, are plotted as the red bands around the original simulated sample, which are shown as the blue lines ("MC"). The data events are shown as black points, with statistical uncertainties indicated by the error bars. In the lower panels of each plot, the ratio of data to simulation is shown with the black points, where the error bars represent the statistical uncertainties in the data. The red-filled area represents the combined statistical and systematic uncertainty in the best fit corrected simulation, shown relative to the nominal prediction as an uncertainty envelope around unity. The gray hatched regions correspond to events that do not enter the selection.

where $\sigma(\mathrm{pp} \to \mathrm{H})$ is the production cross section of the Higgs boson, $\mathcal{B}(\mathrm{H} \to \mathcal{AA} \to 4\gamma)$ is the branching fraction of $\mathrm{H} \to \mathcal{AA} \to 4\gamma$, and $\varepsilon(m_{\mathcal{A}}|m_{\mathrm{H}}\text{-SR} \cap m_{\mathcal{A}}\text{-SR})$ is the efficiency of selection of the $\mathrm{H} \to \mathcal{AA} \to 4\gamma$ events into the final SR, for a given $m_{\mathcal{A}}$ hypothesis. For ease of calculation, we choose a hypothetical signal cross section $\sigma(\mathrm{pp} \to \mathrm{H})\mathcal{B}(\mathrm{H} \to \mathcal{AA} \to 4\gamma) = 1\,\mathrm{pb}$ to normalize the templates. If we consider the SM Higgs boson production cross section $\sigma(\mathrm{pp} \to \mathrm{H}) = 55.6\,\mathrm{pb}$ [59], this is equivalent to $\mathcal{B}(\mathrm{H} \to \mathcal{AA} \to 4\gamma) = 1.8 \times 10^{-2}$. Intermediate signal mass models are constructed by interpolating both the shape and normalization between the generated mass points with $\Delta m_{\mathcal{A}} < 2\,\mathrm{GeV}$, ensuring smooth signal coverage across the full $m_{\mathcal{A}}$ mass range. We validate the interpolation method using generated signal mass points and find the shapes to be comparable. Figure 7 shows the 2D $m_{\mathcal{A}}$ distribution of the signal model from simulation for the $m_{\mathcal{A}} = 5\,\mathrm{GeV}$ hypothesis. The region enclosed by the jagged lines defines the $m_{\mathcal{A}}$-SR region, while the area outside corresponds to the $m_{\mathcal{A}}$-SB region. The 2D $m_{\mathcal{A}}$ distributions are binned using variable bin widths, chosen to maintain sufficient statistical power in each bin. Within this binning scheme, the final template contains 119 bins, with the nominal signal lying along the diagonal within the $m_{\mathcal{A}}$-SR, centered around the expected value of 5 GeV for both axes.

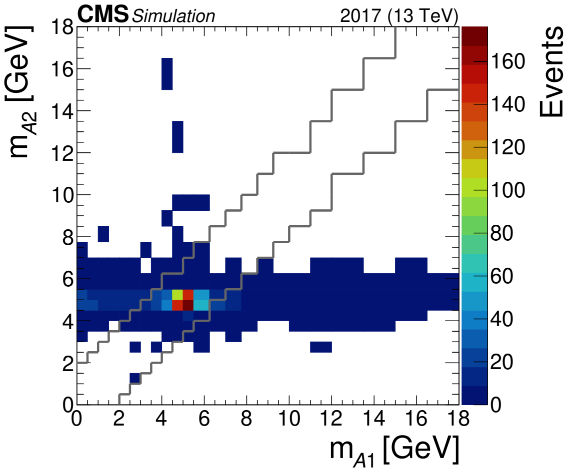

Figure 7. The 2D $m_{\mathcal{A}}$ distribution of the signal model from 2017 simulation for the $m_{\mathcal{A}} = 5\,\text{GeV}$ hypothesis, normalized to $\sigma(\text{pp} \to \text{H})\mathcal{B}(\text{H} \to \mathcal{A}\mathcal{A} \to 4\gamma) = 1\,\text{pb}$. The region enclosed by the jagged lines defines the $m_{\mathcal{A}}$-SR region, while the area outside corresponds to the $m_{\mathcal{A}}$-SB region.

6.2 Background model

The background estimation is performed using data in the SB regions. The shape and yield of the background model are derived by constructing a 2D $m_{\mathcal{A}}$ template, using the data SBs in both the m_{H} and 2D $m_{\mathcal{A}}$ distributions.

To obtain the shape of the background template, we assume that the 2D $m_{\mathcal{A}}$ shape in the m_{H}-SR can be expressed as a linear sum of the corresponding shapes in the m_{H}-SB$_{\text{low}}$ and m_{H}-SB$_{\text{high}}$ regions:

$$p(m_{\mathcal{A}}|m_{\text{H}}\text{-SR}) = f_{\text{SB-low}}\, p(m_{\mathcal{A}}|m_{\text{H}}\text{-SB}_{\text{low}}) + f_{\text{SB-high}}\, p(m_{\mathcal{A}}|m_{\text{H}}\text{-SB}_{\text{high}}), \tag{6.2}$$

where $p(m_{\mathcal{A}}|m_{\text{H}})$ denotes the corresponding 2D $m_{\mathcal{A}}$ shape in each region, with

$$f_{\text{SB-low}} + f_{\text{SB-high}} = 1. \tag{6.3}$$

The $f_{\text{SB-low}}$ ($f_{\text{SB-high}}$) is the relative contribution of the m_{H}-SB$_{\text{low}}$ (m_{H}-SB$_{\text{high}}$) shape to the total shape of the m_{H}-SB, defined as:

$$f_{\text{SB-low}} = \frac{N_{\text{SB-low}}}{N_{\text{SB-low}} + N_{\text{SB-high}}}. \tag{6.4}$$

We then assume that the ratio of the number of events along the 2D $m_{\mathcal{A}}$ diagonal region ($m_{\mathcal{A}}$-SR) derived from m_{H}-SB to the number of events observed in the m_{H}-SR is the same as that in the off-diagonal region ($m_{\mathcal{A}}$-SB):

$$\frac{N(m_{\text{H}}\text{-SR} \cap m_{\mathcal{A}}\text{-SR})}{N(m_{\text{H}}\text{-SB} \cap m_{\mathcal{A}}\text{-SR})} = \frac{N(m_{\text{H}}\text{-SR} \cap m_{\mathcal{A}}\text{-SB})}{N(m_{\text{H}}\text{-SB} \cap m_{\mathcal{A}}\text{-SB})}. \tag{6.5}$$

Taking the ratio from the off-diagonal region, which is signal-depleted by construction, and the on-diagonal yield from the m_{H}-SB, we can obtain a background model for the final SR:

$$N(m_{\text{H}}\text{-SR} \cap m_{\mathcal{A}}\text{-SR}) = \frac{N(m_{\text{H}}\text{-SR} \cap m_{\mathcal{A}}\text{-SB})}{N(m_{\text{H}}\text{-SB} \cap m_{\mathcal{A}}\text{-SB})} N(m_{\text{H}}\text{-SB} \cap m_{\mathcal{A}}\text{-SR}). \tag{6.6}$$

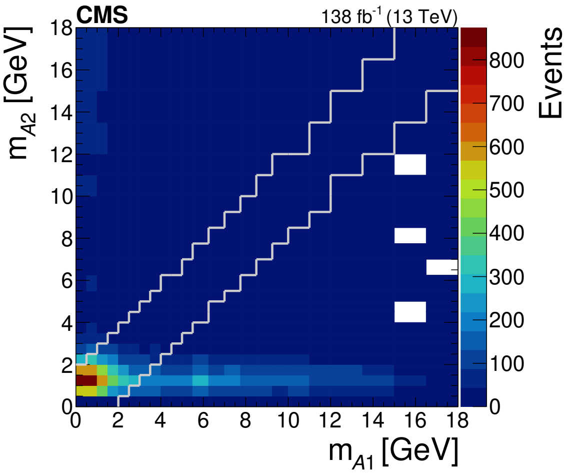

Figure 8. The 2D $m_{\mathcal{A}}$ distribution of the background model constructed from data sidebands. The region enclosed by the jagged lines defines the $m_{\mathcal{A}}$-SR region, while the area outside corresponds to the $m_{\mathcal{A}}$-SB region.

Thus, the final background model for the SR, combining the shape from eq. (6.2) and the yield from eq. (6.6), is:

$$\begin{aligned}\text{bkg}(m_{\text{H}}\text{-SR} \cap m_{\mathcal{A}}\text{-SR}) &= N(m_{\text{H}}\text{-SR} \cap m_{\mathcal{A}}\text{-SR})p(m_{\mathcal{A}}|m_{\text{H}}\text{-SR}) \\ &= N(m_{\text{H}}\text{-SB} \cap m_{\mathcal{A}}\text{-SR})p(m_{\mathcal{A}}|m_{\text{H}}\text{-SB} \cap m_{\mathcal{A}}\text{-SR}) \\ &\times \frac{N(m_{\text{H}}\text{-SR} \cap m_{\mathcal{A}}\text{-SB})}{N(m_{\text{H}}\text{-SB} \cap m_{\mathcal{A}}\text{-SB})}.\end{aligned} \tag{6.7}$$

To visualize the resulting background model, we construct the full 2D $m_{\mathcal{A}}$ distribution using the procedure described above. This distribution, binned using the same variable binning scheme as the signal model, is shown in figure 8. The region enclosed by the jagged lines defines the $m_{\mathcal{A}}$-SR region, while the area outside corresponds to the $m_{\mathcal{A}}$-SB region.

6.2.1 Background model validation

In order to validate the background estimation procedures described above, we compare the expected and observed 2D $m_{\mathcal{A}}$ distribution in the $m_{\mathcal{A}}$-SB regions, where signal contamination was considered but deemed to be negligible. Any residual differences between the two distributions are quantified by fitting the bin-by-bin residuals in the 1D projections along each mass axis with Chebyshev polynomials. The resulting functions are then applied to the nominal 2D background distribution to produce alternative templates, which are used to evaluate the background shape systematic uncertainties discussed in section 7.

The unrolled distribution of the 2D $m_{\mathcal{A}}$ distribution in the $m_{\mathcal{A}}$-SB region is plotted in figure 9. Only bins that belong to the $m_{\mathcal{A}}$-SB region are retained. The unrolling begins at the lower-left corner of the 2D histogram and scans vertically in $m_{\mathcal{A}2}$ at fixed $m_{\mathcal{A}1}$, then steps to the next $m_{\mathcal{A}1}$ column. Bins outside the $m_{\mathcal{A}}$-SB region are skipped, with the x-axis indexing the retained bins in this scanning order. The one-dimensional (1D) projections of the distributions along each $m_{\mathcal{A}}$ axis are also shown in the lower panels. In the upper panel of the plots, the black points are the observed data with error bars corresponding to the statistical uncertainties. The blue line shows the nominal expected background distribution, with the blue shaded region indicating its statistical and systematic uncertainties added in quadrature. In the lower panel, the ratio of the observed data to the nominal expected background is shown as black points, with the error bars corresponding to statistical uncertainties in the former. The ratio of the statistical plus systematic uncertainties in the background over the background model is shown as the blue band. We find good agreement between the data and the background prediction within the uncertainties. In addition, signal injection tests are performed, which do not show any potential bias in the background prediction method for the entire range of signal hypotheses considered. As a further cross-check, the normalization factors in the signal region, that are derived from the combined sidebands, are found to be compatible with those estimated from the low and high sidebands separately. This demonstrates that the 2D $m_{\mathcal{A}}$ shape does not vary significantly across the $m_{\Gamma\Gamma}$ range and residual correlations between $m_{\Gamma\Gamma}$ and the 2D $m_{\mathcal{A}}$ structure do not bias the background estimate.

7 Systematic uncertainties

The dominant uncertainty that affects the extraction of the signal is the statistical uncertainty in the background modeling. In addition, systematic uncertainties related to both the background and signal models are taken into account. For the signal model, alternate templates are generated by shifting the nominal prediction up or down by one standard deviation of each uncertainty source. The following sources are considered:

- *Integrated luminosity.* The uncertainty in the integrated luminosity measurement is 1.2, 2.3, and 2.5% for the 2016, 2017, and 2018 data-taking periods, respectively [60–62], leading to an overall uncertainty of 1.6%. These uncertainties are considered to be partially correlated across the three years.

- *Trigger efficiency.* To account for differences in trigger efficiency between data and simulation, trigger efficiencies in data are derived via the tag-and-probe method [58] using $Z \to e^+e^-$ events. The efficiency estimated in simulation is applied to the signal model, and a systematic uncertainty is assigned to account for potential differences with respect to data. This uncertainty ranges from 20% at $m_{\mathcal{A}} = 1\,\text{GeV}$ to 1% at $m_{\mathcal{A}} = 15\,\text{GeV}$. Larger values are assigned at low $m_{\mathcal{A}}$, where the kinematic phase space of the photon candidates that pass the trigger requirements differs slightly from that used in the standard trigger efficiency measurements. A conservative uncertainty, corresponding to the difference between the trigger efficiency in simulation and that obtained from data measurements, is assigned to ensure full coverage.

- *Photon identification.* Correction factors are applied to the signal model to account for differences in photon identification efficiency between data and simulation, as computed in ref. [21]. These scale factors are obtained with the tag-and-probe procedure using $Z \to e^+e^-$ events, where the smeared electron shower serves as a proxy for merged-photon candidates, directly establishing the validity of this approach for the merged-diphoton topology. The associated uncertainty in this correction ranges from 1 to 3%.

JHEP07(2026)119

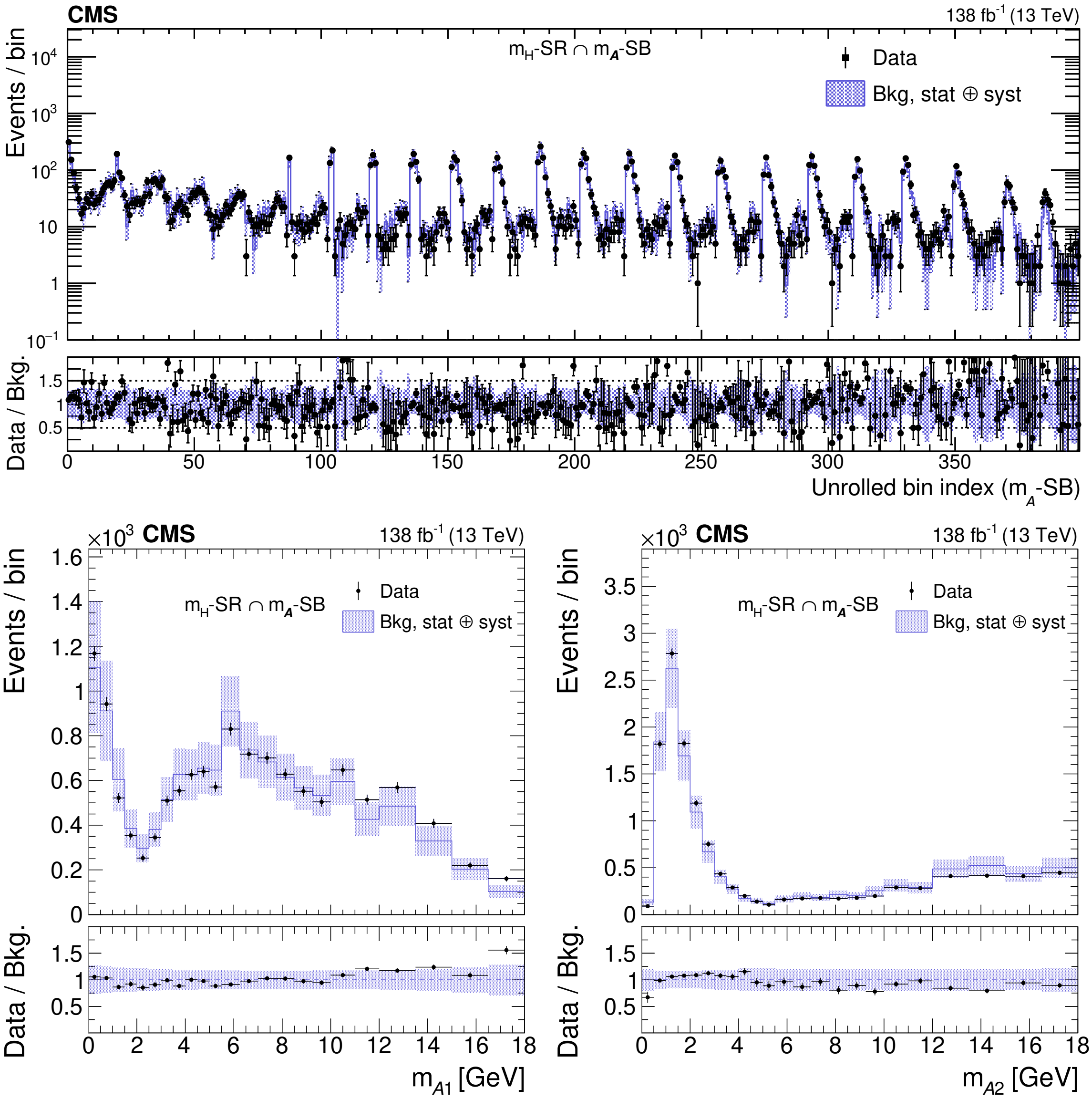

Figure 9. Expected background versus observed data 2D $m_{\mathcal{A}}$ spectra in the m_{H}-SR $\cap$ $m_{\mathcal{A}}$-SB region. Upper plot: unrolled spectra made by scanning along bins of increasing $m_{\mathcal{A}2}$ at fixed $m_{\mathcal{A}1}$ before incrementing in $m_{\mathcal{A}1}$. Only the bins in the $m_{\mathcal{A}}$-SB region are included, with the x-axis corresponding to the unrolled bin index of the selected bins, listed sequentially. Lower plot: projected 1D $m_{\mathcal{A}}$ spectra corresponding to merged (left) and resolved (right) candidates. In the upper panels of each plot, the black points with error bars ("Data") are the observed data values, with the error bars corresponding to statistical uncertainties. The blue line corresponds to the background model, with the blue band corresponding to its statistical uncertainties and systematic uncertainties added in quadrature ("Bkg, stat $\oplus$ syst"). In the lower panel of the same plot, the ratio of the observed data over the estimated background value is shown as black points, with error bars corresponding to statistical uncertainties in the former. The ratio of the statistical plus systematic uncertainties in the background over the background prediction is shown as the blue band.

- *Photon energy scale and resolution.* Corrections are applied to the photon energy scale and resolution in simulation, as computed in ref. [23]. The resulting uncertainty in the signal model is a maximum bin-by-bin variation of $<$3% from the scale and $\sim$0.1% from the resolution.

- *Mass regression scale and smearing.* Following the procedure described in section 5.3, the difference between the mass regression response in data and simulation is accounted for in the signal model by applying a relative scale shift and an additional Gaussian smearing to the simulated regressed mass of each merged-photon candidate. The scale and smearing parameters are determined independently for each data-taking year and each $|\eta|$ category. The best-fit values of the relative scale, $\hat{s}_{\text{scale}}$, and smearing, $\hat{s}_{\text{smear}}$, are obtained by minimizing the χ^2 between the regression response for electrons in data and in simulation after applying the corrections to the simulated distribution. The resulting scale shifts range from 1.6 to 6%, and the additional smearing reaches up to 260 MeV.

For the background model, a systematic uncertainty is assigned to account for potential mismodeling of the expected background shape. As described in section 6.2.1, the residual differences between the observed and expected distributions in the $m_{\mathcal{A}}$-SB region are fitted along each mass axis using Chebyshev polynomials: second order in $m_{\mathcal{A}1}$ and third order in $m_{\mathcal{A}2}$. Each polynomial coefficient defines an independent variation, where the full correction associated with that coefficient is applied as an up or down shift relative to the nominal 2D background template, thereby producing the alternative templates used as the background shape systematic variations in the final fit. The impact of these background modeling uncertainties on the limits is subdominant compared to the statistical uncertainty of the background template.

8 Results

A statistical hypothesis test using a maximum likelihood estimation [63] is performed to extract the best fit between the observed 2D $m_{\mathcal{A}}$ distribution and the constructed signal-plus-background model, $\mu S + B$, where μ is the signal strength parameter for each signal mass point. Systematic and statistical uncertainties from the constructed signal and background models are treated as penalty terms or “nuisance parameters” in the likelihood function. The results of this analysis are used to set upper limits on the product of the production cross section of the Higgs boson and the branching fraction into four photons via a pair of $\mathcal{A}$ particles, $\sigma(\mathrm{H})\mathcal{B}(\mathrm{H} \to \mathcal{A}\mathcal{A} \to 4\gamma)$. The CL_s criterion [64, 65] is used to set the upper limits, using the asymptotic approximation [66]. The results are determined using the CMS statistical analysis tool COMBINE [67].

Figure 10 shows the 2D $m_{\mathcal{A}}$ distribution spectra in the final SR. The upper plot displays the unrolled distribution of the 2D $m_{\mathcal{A}}$ distribution. The unrolling begins at the lower-left corner of the 2D histogram and scans vertically in $m_{\mathcal{A}2}$ at fixed $m_{\mathcal{A}1}$, then steps to the next $m_{\mathcal{A}1}$ column. Bins outside the $m_{\mathcal{A}}$-SR region are skipped, with the x-axis indexing the retained bins in this scanning order. The lower plots show the 1D projections of the 2D $m_{\mathcal{A}}$ distribution onto the $m_{\mathcal{A}1}$ (left) and $m_{\mathcal{A}2}$ (right) axes. The unrolled 2D distribution is chosen as the final discriminant, since the 2D distribution provides better sensitivity than any individual 1D projection. In each of the plots, the background model (in blue), after fitting to the data (in black), is shown overlaid with the signal model distributions for $m_{\mathcal{A}}$ = 3, 10, and 15 GeV. Good agreement between data and background prediction is observed. No statistically significant excess above the SM expectation is found in the explored mass range.

The observed upper limits on the signal cross section times branching fraction $\sigma(\mathrm{pp} \to \mathrm{H})$ $\mathcal{B}$ $(\mathrm{H} \to \mathcal{A}\mathcal{A} \to 4\gamma)$ at 95% CL are plotted with a solid black line, with the median expected limit in a dashed black line, along with the 68 and 95% CL intervals in green and yellow bands, respectively, in figure 11. The 95% CL observed (expected) limits range from a value of 0.264 (0.354) pb for $m_{\mathcal{A}} = 1$ GeV to 0.005 (0.006) pb for $m_{\mathcal{A}} = 15$ GeV. The expected and observed limits are compatible across the full mass range.

Figure 12 presents a comparison of the observed and expected upper limits from previous CMS and ATLAS searches with those obtained in this search. The largest improvement in our search compared to the ATLAS search is achieved at a mass of $m_{\mathcal{A}} = 3$ GeV, where the observed limit is 100 times more stringent than the previous ATLAS result [22]. The ATLAS Collaboration attributes their reduced sensitivity in this region to the transition between the merged and resolved photon categories, where the merged category has significantly larger background contributions. The sensitivity of our search is reduced at the lowest mass compared to the previous CMS search, since the fully merged photon signature still dominates there, while at the highest masses it is reduced because of the small number of events, the use of coarser binning, and the large background uncertainty. This search with the semi-merged photon signatures thus enables the extraction of stringent limits across the entire mass spectrum, bridging the gap in sensitivity between the two previous CMS searches, and is also the first measurement from the CMS experiment in the mass range $m_{\mathcal{A}} = 1$–15 GeV.

9 Summary

A search for the exotic decay of the Higgs boson of the form $\mathrm{H} \to \mathcal{A}\mathcal{A} \to 4\gamma$ in events with three photon-like objects has been performed using proton-proton collision data collected by the CMS experiment at $\sqrt{s} = 13$ TeV corresponding to an integrated luminosity of 138 fb^{-1}. One of the hypothetical particles, $\mathcal{A}$, is assumed to decay promptly to one semi-merged diphoton candidate reconstructed as a single photon-like object, while the other $\mathcal{A}$ decays into a pair of resolved photons. No excess above the estimated background is found. Upper limits are set on the product of the Higgs boson production cross section and branching fraction, $\sigma(\mathrm{pp} \to \mathrm{H})\,\mathcal{B}(\mathrm{H} \to \mathcal{A}\mathcal{A} \to 4\gamma)$, ranging from 0.264 to 0.005 pb at 95% confidence level for masses of $\mathcal{A}$ in the range 1–15 GeV. These limits are the most stringent to date in the 1–5 GeV mass range.

Acknowledgments

We congratulate our colleagues in the CERN accelerator departments for the excellent performance of the LHC and thank the technical and administrative staffs at CERN and at other CMS institutes for their contributions to the success of the CMS effort. In addition, we gratefully acknowledge the computing centers and personnel of the Worldwide LHC Computing

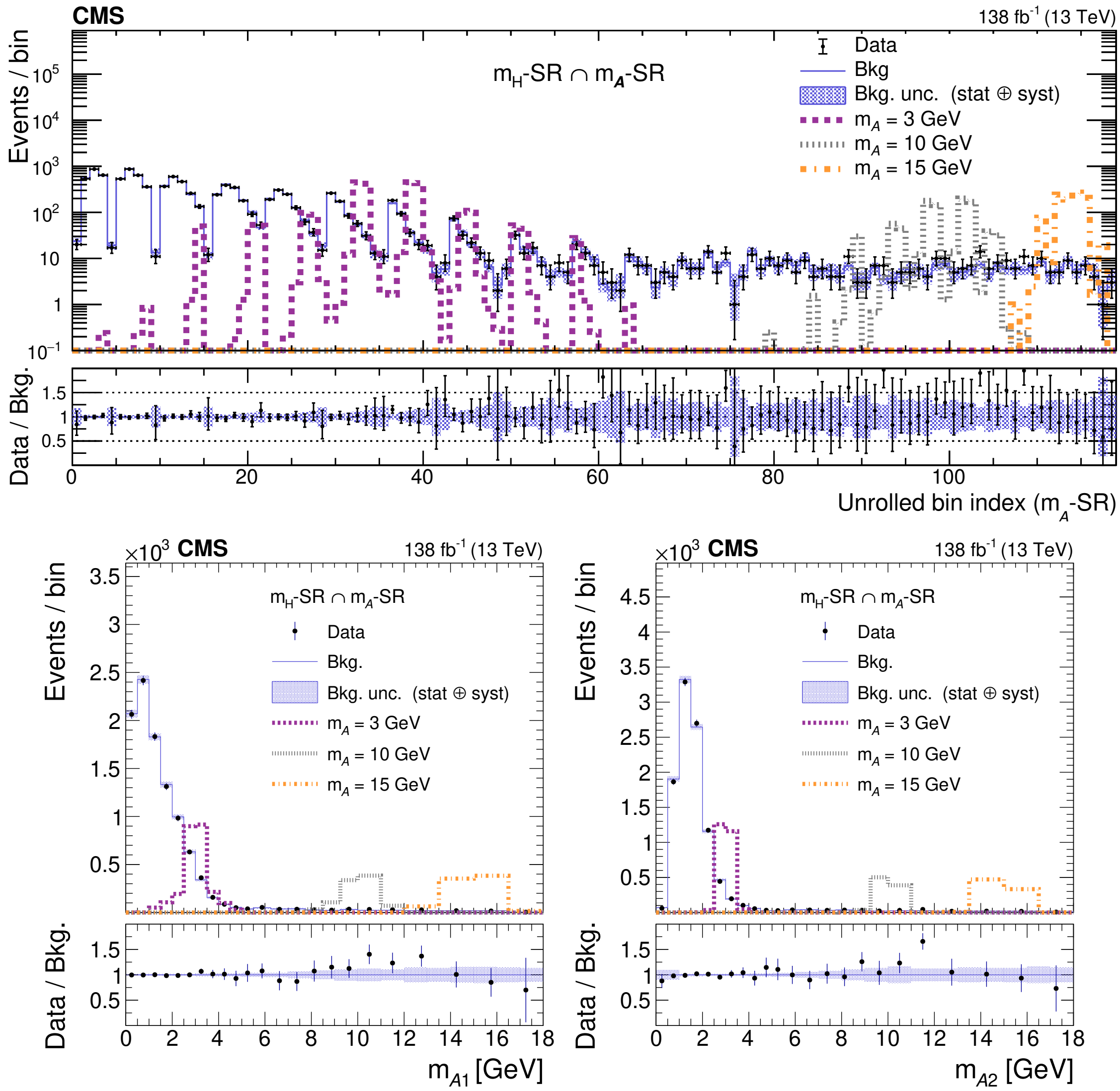

Figure 10. The 2D $m_{\mathcal{A}}$ spectra in the final signal region. Upper plot: The unrolled 2D $m_{\mathcal{A}}$ distribution made by scanning along bins of increasing $m_{\mathcal{A}2}$ at fixed $m_{\mathcal{A}1}$ before incrementing in $m_{\mathcal{A}1}$. Only the bins in the $m_{\mathcal{A}}$-SR region are included, with the x-axis corresponding to the unrolled bin index of the selected bins, listed sequentially. Lower plot: 1D projections on the $m_{\mathcal{A}1}$ (left) and $m_{\mathcal{A}2}$ (right) axes of the 2D $m_{\mathcal{A}}$ distribution. The data distributions (black points) are plotted against the total predicted background distributions (blue curves) after fitting to the data. The statistical plus systematic uncertainties in the background distribution are plotted as the blue band. The corresponding distributions of simulated $\mathrm{H} \to \mathcal{A}\mathcal{A} \to 4\gamma$ events for $m_{\mathcal{A}} = 3$ (purple curve), 10 (gray curve), and 15 GeV (orange curve) are also overlaid on top. They are each normalized to the value of the expected upper limit to the signal cross section times 50. The lower panels of each plot show the ratio of the observed data over the predicted background as the black points, with the error bars representing the statistical uncertainties in the former. The ratio of the statistical plus systematic uncertainties in the background over the background prediction is shown as the blue band.

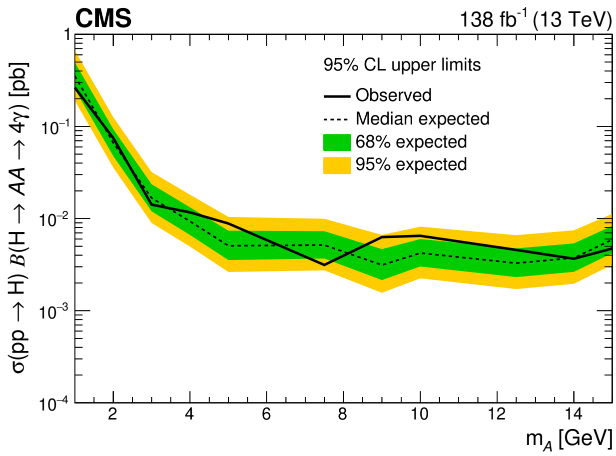

Figure 11. Observed (solid black line) and median expected (dashed black line) upper limits at 95% CL on the signal cross section times branching fraction $\sigma(\mathrm{pp} \to \mathrm{H})\,\mathcal{B}(\mathrm{H} \to \mathcal{AA} \to 4\gamma)$ at various $m_{\mathcal{A}}$ mass points. The 68 and 95% confidence intervals around the median expected limit are shown as the green and yellow bands, respectively.

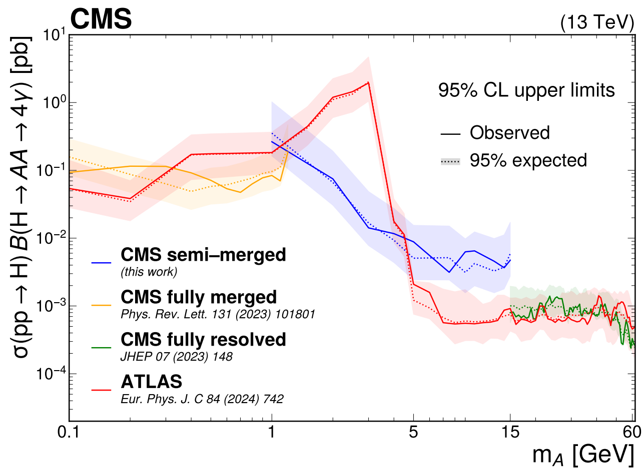

Figure 12. Observed (solid line) and expected (dashed line) upper limits, including the 95% CL interval around the expected limit, from this search (CMS semi-merged) compared to the previous CMS and ATLAS searches [20–22], over the full $m_{\mathcal{A}}$ range of 0.1 to 60 GeV. The limits are shown in terms of $\sigma(\mathrm{pp} \to \mathrm{H})\,\mathcal{B}(\mathrm{H} \to \mathcal{AA} \to 4\gamma)$.

Grid and other centers for delivering so effectively the computing infrastructure essential to our analyses. Finally, we acknowledge the enduring support for the construction and operation of the LHC, the CMS detector, and the supporting computing infrastructure provided by the following funding agencies: SC (Armenia), BMBWF and FWF (Austria); FNRS and FWO (Belgium); CNPq, CAPES, FAPERJ, FAPERGS, and FAPESP (Brazil); MES and BNSF (Bulgaria); CERN; CAS, MoST, and NSFC (China); MINCIENCIAS (Colombia); MSES and CSF (Croatia); RIF (Cyprus); SENESCYT (Ecuador); ERC PRG, TARISTU24-TK10 and MoER TK202 (Estonia); Academy of Finland, MEC, and HIP (Finland); CEA and CNRS/IN2P3 (France); SRNSF (Georgia); BMFTR, DFG, and HGF (Germany); GSRI

JHEP07(2026)119

(Greece); NKFIH (Hungary); DAE and DST (India); IPM (Iran); SFI (Ireland); INFN (Italy); MSIT and NRF (Republic of Korea); MES (Latvia); LMTLT (Lithuania); MOE and UM (Malaysia); BUAP, CINVESTAV, CONACYT, LNS, SEP, and UASLP-FAI (Mexico); MOS (Montenegro); MBIE (New Zealand); PAEC (Pakistan); MES, NSC, and NAWA (Poland); FCT (Portugal); MESTD (Serbia); MICIU/AEI and PCTI (Spain); MOSTR (Sri Lanka); Swiss Funding Agencies (Switzerland); MST (Taipei); MHESI (Thailand); TUBITAK and TENMAK (Türkiye); NASU (Ukraine); STFC (United Kingdom); DOE and NSF (U.S.A.).

Individuals have received support from the Marie-Curie program and the European Research Council and Horizon 2020 Grant, contract Nos. 675440, 724704, 752730, 758316, 765710, 824093, 101115353, 101002207, 101001205, and COST Action CA16108 (European Union); the Leventis Foundation; the Alfred P. Sloan Foundation; the Alexander von Humboldt Foundation; the Science Committee, project no. 22rl-037 (Armenia); the Fonds pour la Formation à la Recherche dans l'Industrie et dans l'Agriculture (FRIA) and Fonds voor Wetenschappelijk Onderzoek contract No. 1228724N (Belgium); the Beijing Municipal Science & Technology Commission, No. Z191100007219010, the Fundamental Research Funds for the Central Universities, the Ministry of Science and Technology of China under Grant No. 2023YFA1605804, the Natural Science Foundation of China under Grant No. 12061141002, 12535004, and USTC Research Funds of the Double First-Class Initiative No. YD2030002017 (China); the Ministry of Education, Youth and Sports (MEYS) of the Czech Republic; the Shota Rustaveli National Science Foundation, grant FR-22-985 (Georgia); the Deutsche Forschungsgemeinschaft (DFG), among others, under Germany's Excellence Strategy – EXC 2121 "Quantum Universe" – 390833306, and under project number 400140256 – GRK2497; the Hellenic Foundation for Research and Innovation (HFRI), Project Number 2288 (Greece); the Hungarian Academy of Sciences, the New National Excellence Program – ÚNKP, the NKFIH research grants K 131991, K 133046, K 138136, K 143460, K 143477, K 146913, K 146914, K 147048, 2020-2.2.1-ED-2021-00181, TKP2021-NKTA-64, and 2025-1.1.5-NEMZ_KI-2025-00004 (Hungary); the Council of Science and Industrial Research, India; ICSC – National Research Center for High Performance Computing, Big Data and Quantum Computing, FAIR – Future Artificial Intelligence Research, and CUP I53D23001070006 (Mission 4 Component 1), funded by the NextGenerationEU program (Italy); the Latvian Council of Science; the Ministry of Education and Science, project no. 2022/WK/14, and the National Science Center, contracts Opus 2021/41/B/ST2/01369, 2021/43/B/ST2/01552, 2023/49/B/ST2/03273, and the NAWA contract BPN/PPO/2021/1/00011 (Poland); the Fundação para a Ciência e a Tecnologia, grant CEECIND/01334/2018 (Portugal); the National Priorities Research Program by Qatar National Research Fund; MICIU/AEI/10.13039/501100011033, ERDF/EU, "European Union NextGenerationEU/PRTR", and Programa Severo Ochoa del Principado de Asturias (Spain); the Chulalongkorn Academic into Its 2nd Century Project Advancement Project, the National Science, Research and Innovation Fund program IND_FF_68_369_2300_097, and the Program Management Unit for Human Resources & Institutional Development, Research and Innovation, grant B39G680009 (Thailand); the Kavli Foundation; the Nvidia Corporation; the SuperMicro Corporation; the Welch Foundation, contract C-1845; and the Weston Havens Foundation (U.S.A.).

Data Availability Statement. Release and preservation of data used by the CMS Collaboration as the basis for publications is guided by the CMS data preservation, re-use and open access policy.

Code Availability Statement. The CMS core software is publicly available on GitHub.

References

[1] L. Evans and P. Bryant, *LHC Machine*, 2008 *JINST* **3** S08001 [INSPIRE].

[2] ATLAS collaboration, *Observation of a new particle in the search for the Standard Model Higgs boson with the ATLAS detector at the LHC*, *Phys. Lett. B* **716** (2012) 1 [arXiv:1207.7214] [INSPIRE].

[3] CMS collaboration, *Observation of a New Boson at a Mass of 125 GeV with the CMS Experiment at the LHC*, *Phys. Lett. B* **716** (2012) 30 [arXiv:1207.7235] [INSPIRE].

[4] CMS collaboration, *Observation of a New Boson with Mass Near 125 GeV in pp Collisions at* $\sqrt{s} = 7$ *and* 8 *TeV*, *JHEP* **06** (2013) 081 [arXiv:1303.4571] [INSPIRE].

[5] CMS collaboration, *Combined measurements and interpretations of Higgs boson production and decay in proton-proton collisions at* $\sqrt{s} = 13$ *TeV*, CMS-HIG-21-018 CERN-EP-2026-009 [arXiv:2602.18611] [INSPIRE].

[6] D. Curtin et al., *Exotic decays of the 125 GeV Higgs boson*, *Phys. Rev. D* **90** (2014) 075004 [arXiv:1312.4992] [INSPIRE].

[7] D. Curtin, R. Essig, S. Gori and J. Shelton, *Illuminating Dark Photons with High-Energy Colliders*, *JHEP* **02** (2015) 157 [arXiv:1412.0018] [INSPIRE].

[8] F. Chadha-Day, J. Ellis and D.J.E. Marsh, *Axion dark matter: What is it and why now?*, *Sci. Adv.* **8** (2022) abj3618 [arXiv:2105.01406] [INSPIRE].

[9] R.D. Peccei and H.R. Quinn, *CP Conservation in the Presence of Instantons*, *Phys. Rev. Lett.* **38** (1977) 1440 [INSPIRE].

[10] M. Bauer, M. Neubert and A. Thamm, *Collider Probes of Axion-Like Particles*, *JHEP* **12** (2017) 044 [arXiv:1708.00443] [INSPIRE].

[11] R.D. Peccei, *The strong CP problem and axions*, *Lect. Notes Phys.* **741** (2008) 3 [hep-ph/0607268] [INSPIRE].

[12] CMS collaboration, *Search for exotic decays of the Higgs boson to a pair of pseudoscalars in the* $\mu\mu bb$ *and* $\tau\tau bb$ *final states*, *Eur. Phys. J. C* **84** (2024) 493 [arXiv:2402.13358] [INSPIRE].

[13] CMS collaboration, *Search for the decay of the Higgs boson to a pair of light pseudoscalar bosons in the final state with four bottom quarks in proton-proton collisions at* $\sqrt{s} = 13$ *TeV*, *JHEP* **06** (2024) 097 [arXiv:2403.10341] [INSPIRE].

[14] CMS collaboration, *Search for light pseudoscalar boson pairs produced from Higgs boson decays using the* 4τ *and* $2\mu 2\tau$ *final states in proton-proton collisions at* $\sqrt{s} = 13$ *TeV*, *JHEP* **04** (2026) 132 [arXiv:2508.06947] [INSPIRE].

[15] ATLAS collaboration, *Search for Higgs boson exotic decays into Lorentz-boosted light bosons in the four-τ final state at $\sqrt{s} = 13$ TeV with the ATLAS detector*, *Phys. Lett. B* **870** (2025) 139843 [arXiv:2503.05463] [INSPIRE].

[16] CMS collaboration, *Search for light long-lived particles decaying to displaced jets in proton–proton collisions at $\sqrt{s} = 13.6$ TeV*, *Rept. Prog. Phys.* **88** (2025) 037801 [arXiv:2409.10806] [INSPIRE].

[17] CMS collaboration, *A search for pair production of new light bosons decaying into muons in proton-proton collisions at 13 TeV*, *Phys. Lett. B* **796** (2019) 131 [arXiv:1812.00380] [INSPIRE].

[18] CMS collaboration, *Particle-flow reconstruction and global event description with the CMS detector*, 2017 *JINST* **12** P10003 [arXiv:1706.04965] [INSPIRE].

[19] CMS collaboration, *Reconstruction of decays to merged photons using end-to-end deep learning with domain continuation in the CMS detector*, *Phys. Rev. D* **108** (2023) 052002 [arXiv:2204.12313] [INSPIRE].

[20] CMS collaboration, *Search for the exotic decay of the Higgs boson into two light pseudoscalars with four photons in the final state in proton-proton collisions at $\sqrt{s} = 13$ TeV*, *JHEP* **07** (2023) 148 [arXiv:2208.01469] [INSPIRE].

[21] CMS collaboration, *Search for exotic Higgs boson decays $H \to \mathcal{AA} \to 4\gamma$ with events containing two merged diphotons in proton-proton collisions at $\sqrt{s} = 13$ TeV*, *Phys. Rev. Lett.* **131** (2023) 101801 [arXiv:2209.06197] [INSPIRE].

[22] ATLAS collaboration, *Search for short- and long-lived axion-like particles in $H \to aa \to 4\gamma$ decays with the ATLAS experiment at the LHC*, *Eur. Phys. J. C* **84** (2024) 742 [arXiv:2312.03306] [INSPIRE].

[23] CMS collaboration, *Electron and photon reconstruction and identification with the CMS experiment at the CERN LHC*, 2021 *JINST* **16** P05014 [arXiv:2012.06888] [INSPIRE].

[24] HEPData record for this analysis, DOI:10.17182/hepdata.166011.

[25] CMS collaboration, *The CMS Experiment at the CERN LHC*, 2008 *JINST* **3** S08004 [INSPIRE].

[26] CMS collaboration, *Development of the CMS detector for the CERN LHC Run 3*, 2024 *JINST* **19** P05064 [arXiv:2309.05466] [INSPIRE].

[27] CMS collaboration, *Performance of the CMS Level-1 trigger in proton-proton collisions at $\sqrt{s} = 13$ TeV*, 2020 *JINST* **15** P10017 [arXiv:2006.10165] [INSPIRE].

[28] CMS collaboration, *The CMS trigger system*, 2017 *JINST* **12** P01020 [arXiv:1609.02366] [INSPIRE].

[29] CMS collaboration, *Performance of the CMS high-level trigger during LHC Run 2*, 2024 *JINST* **19** P11021 [arXiv:2410.17038] [INSPIRE].

[30] CMS collaboration, *Performance of the CMS muon detector and muon reconstruction with proton-proton collisions at $\sqrt{s} = 13$ TeV*, 2018 *JINST* **13** P06015 [arXiv:1804.04528] [INSPIRE].

[31] CMS collaboration, *Description and Performance of Track and Primary-Vertex Reconstruction with the CMS Tracker*, 2014 *JINST* **9** P10009 [arXiv:1405.6569] [INSPIRE].

[32] CMS collaboration, *Performance of reconstruction and identification of τ leptons decaying to hadrons and ν_τ in pp collisions at $\sqrt{s} = 13$ TeV*, 2018 *JINST* **13** P10005 [arXiv:1809.02816] [INSPIRE].

[33] CMS collaboration, *Jet energy scale and resolution in the CMS experiment in pp collisions at 8 TeV*, 2017 *JINST* **12** P02014 [arXiv:1607.03663] [INSPIRE].

[34] CMS collaboration, *Performance of missing transverse momentum reconstruction in proton-proton collisions at $\sqrt{s} = 13$ TeV using the CMS detector*, 2019 *JINST* **14** P07004 [arXiv:1903.06078] [INSPIRE].

[35] CMS collaboration, *Pileup mitigation at CMS in 13 TeV data*, 2020 *JINST* **15** P09018 [arXiv:2003.00503] [INSPIRE].

[36] J. Alwall et al., *The automated computation of tree-level and next-to-leading order differential cross sections, and their matching to parton shower simulations*, *JHEP* **07** (2014) 079 [arXiv:1405.0301] [INSPIRE].

[37] NNPDF collaboration, *Parton distributions from high-precision collider data*, *Eur. Phys. J. C* **77** (2017) 663 [arXiv:1706.00428] [INSPIRE].

[38] T. Sjöstrand et al., *An introduction to PYTHIA 8.2*, *Comput. Phys. Commun.* **191** (2015) 159 [arXiv:1410.3012] [INSPIRE].

[39] CMS collaboration, *Extraction and validation of a new set of CMS PYTHIA8 tunes from underlying-event measurements*, *Eur. Phys. J. C* **80** (2020) 4 [arXiv:1903.12179] [INSPIRE].

[40] GEANT4 collaboration, *GEANT4 — A Simulation Toolkit*, *Nucl. Instrum. Meth. A* **506** (2003) 250 [INSPIRE].

[41] CMS collaboration, *Search for a standard model-like Higgs boson in the mass range between 70 and 110 GeV in the diphoton final state in proton-proton collisions at $\sqrt{s} = 13$ TeV*, *Phys. Lett. B* **860** (2025) 139067 [arXiv:2405.18149] [INSPIRE].

[42] ATLAS collaboration, *Jet reconstruction and performance using particle flow with the ATLAS Detector*, *Eur. Phys. J. C* **77** (2017) 466 [arXiv:1703.10485] [INSPIRE].

[43] CMS collaboration, *Observation of the Diphoton Decay of the Higgs Boson and Measurement of Its Properties*, *Eur. Phys. J. C* **74** (2014) 3076 [arXiv:1407.0558] [INSPIRE].

[44] CMS collaboration, *Performance of photon reconstruction and identification with the CMS detector in proton-proton collisions at $\sqrt{s} = 8$ TeV*, 2015 *JINST* **10** P08010 [arXiv:1502.02702] [INSPIRE].

[45] X. Ju and B. Nachman, *Supervised Jet Clustering with Graph Neural Networks for Lorentz Boosted Bosons*, *Phys. Rev. D* **102** (2020) 075014 [arXiv:2008.06064] [INSPIRE].

[46] ATLAS collaboration, *Performance of top-quark and W-boson tagging with ATLAS in Run 2 of the LHC*, *Eur. Phys. J. C* **79** (2019) 375 [arXiv:1808.07858] [INSPIRE].

[47] P.T. Komiske, E.M. Metodiev and J. Thaler, *Energy Flow Networks: Deep Sets for Particle Jets*, *JHEP* **01** (2019) 121 [arXiv:1810.05165] [INSPIRE].

[48] S. Ghosh et al., *A simulation study to distinguish prompt photon from π^0 and beam halo in a granular calorimeter using deep networks*, 2019 *JINST* **14** P01011 [arXiv:1808.03987] [INSPIRE].

[49] L. Uboldi et al., *Extracting low energy signals from raw LArTPC waveforms using deep learning techniques — A proof of concept*, *Nucl. Instrum. Meth. A* **1028** (2022) 166371 [arXiv:2106.09911] [INSPIRE].

[50] M. Andrews et al., *End-to-end jet classification of quarks and gluons with the CMS Open Data*, *Nucl. Instrum. Meth. A* **977** (2020) 164304 [arXiv:1902.08276] [INSPIRE].

[51] MicroBooNE collaboration, *Deep neural network for pixel-level electromagnetic particle identification in the MicroBooNE liquid argon time projection chamber*, *Phys. Rev. D* **99** (2019) 092001 [arXiv:1808.07269] [INSPIRE].

JHEP07(2026)119

[52] Exa.TrkX collaboration, *Graph Neural Networks for Particle Reconstruction in High Energy Physics detectors*, in the proceedings of the *33rd Annual Conference on Neural Information Processing Systems*, Vancouver, Canada, December 08–14 (2019) [arXiv:2003.11603] [INSPIRE].

[53] CMS collaboration, *Mini-AOD: A New Analysis Data Format for CMS*, *J. Phys. Conf. Ser.* **664** (2015) 072052 [arXiv:1702.04685] [INSPIRE].

[54] CMS collaboration, *The NanoAOD event data format in CMS*, *J. Phys. Conf. Ser.* **1525** (2020) 012038 [INSPIRE].

[55] L. Gray, T. Klijnsma and S. Ghosh, *A Dynamic Reduction Network for Point Clouds*, arXiv:2003.08013 [INSPIRE].

[56] I. Goodfellow, Y. Bengio and A. Courville, *Deep Learning*, MIT Press (2016).

[57] Y. Wang et al., *Dynamic Graph CNN for Learning on Point Clouds*, arXiv:1801.07829 [INSPIRE].

[58] CMS collaboration, *Measurement of the Inclusive W and Z Production Cross Sections in pp Collisions at* $\sqrt{s} = 7$ *TeV*, *JHEP* **10** (2011) 132 [arXiv:1107.4789] [INSPIRE].

[59] LHC Higgs Cross Section Working Group collaboration, *Handbook of LHC Higgs Cross Sections: 4. Deciphering the Nature of the Higgs Sector*, *CERN Yellow Rep. Monogr.* **2** (2017) 1 [arXiv:1610.07922] [INSPIRE].

[60] CMS collaboration, *Precision luminosity measurement in proton-proton collisions at* $\sqrt{s} = 13$ *TeV in 2015 and 2016 at CMS*, *Eur. Phys. J. C* **81** (2021) 800 [arXiv:2104.01927] [INSPIRE].

[61] CMS collaboration, *CMS luminosity measurement for the 2017 data-taking period at* $\sqrt{s} = 13$ *TeV*, CMS-PAS-LUM-17-004.

[62] CMS collaboration, *CMS luminosity measurement for the 2018 data-taking period at* $\sqrt{s} = 13$ *TeV*, CMS-PAS-LUM-18-002.

[63] ATLAS et al. collaborations, *Procedure for the LHC Higgs boson search combination in Summer 2011*, CMS-NOTE-2011-005 [INSPIRE].

[64] T. Junk, *Confidence level computation for combining searches with small statistics*, *Nucl. Instrum. Meth. A* **434** (1999) 435 [hep-ex/9902006] [INSPIRE].

[65] A.L. Read, *Presentation of search results: The* CL_s *technique*, *J. Phys. G* **28** (2002) 2693 [INSPIRE].

[66] G. Cowan, K. Cranmer, E. Gross and O. Vitells, *Asymptotic formulae for likelihood-based tests of new physics*, *Eur. Phys. J. C* **71** (2011) 1554 [*Erratum ibid.* **73** (2013) 2501] [arXiv:1007.1727] [INSPIRE].

[67] CMS collaboration, *The CMS Statistical Analysis and Combination Tool: Combine*, *Comput. Softw. Big Sci.* **8** (2024) 19 [arXiv:2404.06614] [INSPIRE].

The CMS collaboration

A. Hayrapetyan[1], V. Makarenko[1], A. Tumasyan[1,a], W. Adam[2], J.W. Andrejkovic[2], L. Benato[2], T. Bergauer[2], M. Dragicevic[2], C. Giordano[2], P.S. Hussain[2], M. Jeitler[2,b], N. Krammer[2], A. Li[2], D. Liko[2], M. Matthewman[2], I. Mikulec[2], J. Schieck[2,b], R. Schöfbeck[2,b], D. Schwarz[2], M. Shooshtari[2], M. Sonawane[2], W. Waltenberger[2], C.-E. Wulz[2,b], T. Janssen[3], H. Kwon[3], D. Ocampo Henao[3], T. Van Laer[3], P. Van Mechelen[3], J. Bierkens[4], N. Breugelmans[4], J. D'Hondt[4], S. Dansana[4], A. De Moor[4], M. Delcourt[4], F. Heyen[4], Y. Hong[4], P. Kashko[4], S. Lowette[4], I. Makarenko[4], D. Müller[4], J. Song[4], S. Tavernier[4], M. Tytgat[4,c], G.P. Van Onsem[4], S. Van Putte[4], D. Vannerom[4], B. Bilin[5], B. Clerbaux[5], A.K. Das[5], I. De Bruyn[5], G. De Lentdecker[5], H. Evard[5], L. Favart[5], P. Gianneios[5], A. Khalilzadeh[5], F.A. Khan[5], A. Malara[5], M.A. Shahzad[5], L. Thomas[5], M. Vanden Bemden[5], C. Vander Velde[5], P. Vanlaer[5], F. Zhang[5], M. De Coen[6], D. Dobur[6], G. Gokbulut[6], J. Knolle[6], D. Marckx[6], K. Skovpen[6], A.M. Tomaru[6], N. Van Den Bossche[6], J. van der Linden[6], J. Vandenbroeck[6], L. Wezenbeek[6], S. Bein[7], A. Benecke[7], A. Bethani[7], G. Bruno[7], A. Cappati[7], J. De Favereau De Jeneret[7], C. Delaere[7], F. Gameiro Casalinho[7], A. Giammanco[7], A.O. Guzel[7], V. Lemaitre[7], J. Lidrych[7], P. Malek[7], P. Mastrapasqua[7], S. Turkcapar[7], G.A. Alves[8], M. Barroso Ferreira Filho[8], E. Coelho[8], C. Hensel[8], T. Menezes De Oliveira[8], C. Mora Herrera[8], P. Rebello Teles[8], M. Soeiro[8], E.J. Tonelli Manganote[8,d], A. Vilela Pereira[8,e], W.L. Aldá Júnior[9], H. Brandao Malbouisson[9], W. Carvalho[9], J. Chinellato[9,f], M. Costa Reis[9], E.M. Da Costa[9], G.G. Da Silveira[9,g], D. De Jesus Damiao[9], S. Fonseca De Souza[9], R. Gomes De Souza[9], S. S. Jesus[9], T. Laux Kuhn[9,g], M. Macedo[9], K. Mota Amarilo[9], L. Mundim[9], H. Nogima[9], J.P. Pinheiro[9], A. Santoro[9], A. Sznajder[9], M. Thiel[9], F. Torres Da Silva De Araujo[9,h], C.A. Bernardes[10,g], F. Damas[10], T.R. Fernandez Perez Tomei[10], E.M. Gregores[10], B. Lopes Da Costa[10], I. Maietto Silverio[10], P.G. Mercadante[10], S.F. Novaes[10], B. Orzari[10], Sandra S. Padula[10], V. Scheurer[10], A. Aleksandrov[11], G. Antchev[11], P. Danev[11], R. Hadjiiska[11], P. Iaydjiev[11], M. Shopova[11], G. Sultanov[11], A. Dimitrov[12], L. Litov[12], B. Pavlov[12], P. Petkov[12], A. Petrov[12], S. Keshri[13], D. Laroze[13], S. Thakur[13], W. Brooks[14], T. Cheng[15], T. Javaid[15], L. Wang[15], L. Yuan[15], Z. Hu[16], Z. Liang[16], J. Liu[16], X. Wang[16], H. Yang[16], G.M. Chen[17,i], H.S. Chen[17,i], M. Chen[17,i], Y. Chen[17], Q. Hou[17], X. Hou[17], F. Iemmi[17], C.H. Jiang[17], A. Kapoor[17,j], H. Liao[17], G. Liu[17], Z.-A. Liu[17,k], J.N. Song[17,k], S. Song[17], J. Tao[17], C. Wang[17,i], J. Wang[17], H. Zhang[17], J. Zhao[17], A. Agapitos[18], Y. Ban[18], A. Carvalho Antunes De Oliveira[18], S. Deng[18], B. Guo[18], Q. Guo[18], C. Jiang[18], A. Levin[18], C. Li[18], Q. Li[18], Y. Mao[18], S. Qian[18], S.J. Qian[18], X. Qin[18], C. Quaranta[18], X. Sun[18], D. Wang[18], J. Wang[18], M. Zhang[18], Y. Zhao[18], C. Zhou[18], S. Yang[19], Z. You[20], K. Jaffel[21], N. Lu[21], G. Bauer[22,l,m], Z. Cui[22,m], B. Li[22,n], H. Wang[22], K. Yi[22,o], J. Zhang[22], Y. Li[23], Z. Lin[24], C. Lu[24], M. Xiao[24,p], C. Avila[25], D.A. Barbosa Trujillo[25], A. Cabrera[25], C. Florez[25], J. Fraga[25], J.A. Reyes Vega[25], C. Rendón[26], M. Rodriguez[26], A.A. Ruales Barbosa[26], J.D. Ruiz Alvarez[26], N. Godinovic[27], D. Lelas[27], A. Sculac[27], M. Kovac[28], A. Petkovic[28], T. Sculac[28], P. Bargassa[29], V. Brigljevic[29], B.K. Chitroda[29], D. Ferencek[29], K. Jakovcic[29], A. Starodumov[29], T. Susa[29], A. Attikis[30], K. Christoforou[30],

JHEP07(2026)119

C. Leonidou[30], C. Nicolaou[30], L. Paizanos[30], F. Ptochos[30], P.A. Razis[30], H. Rykaczewski[30], H. Saka[30], A. Stepennov[30], M. Finger[31,†], M. Finger Jr.[31], E. Ayala[32], E. Carrera Jarrin[33], S. Khalil[34,q], E. Salama[34,r,s], A. Hussein[35], H. Mohammed[35], K. Ehataht[36], M. Kadastik[36], T. Lange[36], C. Nielsen[36], J. Pata[36], M. Raidal[36], N. Seeba[36], L. Tani[36], E. Brücken[37], A. Milieva[37], K. Osterberg[37], M. Voutilainen[37], F. Garcia[38], P. Inkaew[38], K.T.S. Kallonen[38], R. Kumar Verma[38], T. Lampén[38], K. Lassila-Perini[38], B. Lehtela[38], S. Lehti[38], T. Lindén[38], N.R. Mancilla Xinto[38], M. Myllymäki[38], M.m. Rantanen[38], S. Saariokari[38], N.T. Toikka[38], J. Tuominiemi[38], N. Bin Norjoharuddeen[39], H. Kirschenmann[39], P. Luukka[39], H. Petrow[39], M. Besancon[40], F. Couderc[40], M. Dejardin[40], D. Denegri[40], P. Devouge[40], J.L. Faure[40], F. Ferri[40], P. Gaigne[40], S. Ganjour[40], P. Gras[40], G. Hamel de Monchenault[40], M. Kumar[40], V. Lohezic[40], Y. Maidannyk[40], J. Malcles[40], F. Orlandi[40], L. Portales[40], S. Ronchi[40], M.Ö. Sahin[40], A. Savoy-Navarro[40,t], P. Simkina[40], M. Titov[40], M. Tornago[40], R. Amella Ranz[41], F. Beaudette[41], G. Boldrini[41], P. Busson[41], C. Charlot[41], M. Chiusi[41], T.D. Cuisset[41], O. Davignon[41], A. De Wit[41], T. Debnath[41], I.T. Ehle[41], S. Ghosh[41], A. Gilbert[41], R. Granier de Cassagnac[41], L. Kalipoliti[41], M. Manoni[41], M. Nguyen[41], S. Obraztsov[41], C. Ochando[41], R. Salerno[41], J.B. Sauvan[41], Y. Sirois[41], G. Sokmen[41], L. Urda Gómez[41], A. Zabi[41], A. Zghiche[41], J.-L. Agram[42,u], J. Andrea[42], D. Bloch[42], J.-M. Brom[42], E.C. Chabert[42], C. Collard[42], G. Coulon[42], S. Falke[42], U. Goerlach[42], R. Haeberle[42], A.-C. Le Bihan[42], M. Meena[42], O. Poncet[42], G. Saha[42], P. Vaucelle[42], A. Di Florio[43], D. Amram[44], S. Beauceron[44], B. Blancon[44], G. Boudoul[44], N. Chanon[44], D. Contardo[44], P. Depasse[44], H. El Mamouni[44], J. Fay[44], S. Gascon[44], M. Gouzevitch[44], C. Greenberg[44], G. Grenier[44], B. Ille[44], E. Jourd'Huy[44], M. Lethuillier[44], B. Massoteau[44], L. Mirabito[44], A. Purohit[44], M. Vander Donckt[44], J. Xiao[44], A. Khvedelidze[45,v], I. Lomidze[45], Z. Tsamalaidze[45,v], V. Botta[46], S. Consuegra Rodríguez[46], L. Feld[46], K. Klein[46], M. Lipinski[46], D. Meuser[46], P. Nattland[46], V. Oppenländer[46], A. Pauls[46], D. Pérez Adán[46], N. Röwert[46], M. Teroerde[46], C. Daumann[47], S. Diekmann[47], A. Dodonova[47], N. Eich[47], D. Eliseev[47], F. Engelke[47], J. Erdmann[47], M. Erdmann[47], B. Fischer[47], T. Hebbeker[47], K. Hoepfner[47], F. Ivone[47], A. Jung[47], N. Kumar[47], M.y. Lee[47], F. Mausolf[47], M. Merschmeyer[47], A. Meyer[47], F. Nowotny[47], A. Pozdnyakov[47], W. Redjeb[47], H. Reithler[47], U. Sarkar[47], V. Sarkisovi[47], A. Schmidt[47], C. Seth[47], A. Sharma[47], J.L. Spah[47], V. Vaulin[47], S. Zaleski[47], M.R. Beckers[48], C. Dziwok[48], G. Flügge[48], N. Hoeflich[48], T. Kress[48], A. Nowack[48], O. Pooth[48], A. Stahl[48], A. Zotz[48], H. Aarup Petersen[49], A. Abel[49], M. Aldaya Martin[49], J. Alimena[49], S. Amoroso[49], Y. An[49], I. Andreev[49], J. Bach[49], S. Baxter[49], M. Bayatmakou[49], H. Becerril Gonzalez[49], O. Behnke[49], A. Belvedere[49], F. Blekman[49,w], K. Borras[49,x], A. Campbell[49], S. Chatterjee[49], L.X. Coll Saravia[49], G. Eckerlin[49], D. Eckstein[49], E. Gallo[49,w], A. Geiser[49], V. Guglielmi[49], M. Guthoff[49], A. Hinzmann[49], L. Jeppe[49], M. Kasemann[49], C. Kleinwort[49], R. Kogler[49], M. Komm[49], D. Krücker[49], W. Lange[49], D. Leyva Pernia[49], K.-Y. Lin[49], K. Lipka[49,y], W. Lohmann[49,z], J. Malvaso[49], R. Mankel[49], I.-A. Melzer-Pellmann[49], M. Mendizabal Morentin[49], A.B. Meyer[49], G. Milella[49], K. Moral Figueroa[49], A. Mussgiller[49], L.P. Nair[49], J. Niedziela[49], A. Nürnberg[49], J. Park[49], E. Ranken[49], A. Raspereza[49], D. Rastorguev[49], L. Rygaard[49],

JHEP07(2026)119

M. Scham[49,aa,ab], S. Schnake[49,x], P. Schütze[49], C. Schwanenberger[49,w], D. Selivanova[49], K. Sharko[49], M. Shchedrolosiev[49], D. Stafford[49], M. Torkian[49], F. Vazzoler[49], A. Ventura Barroso[49], R. Walsh[49], D. Wang[49], Q. Wang[49], K. Wichmann[49], L. Wiens[49,x], C. Wissing[49], Y. Yang[49], S. Zakharov[49], A. Zimermmane Castro Santos[49], A.R. Alves Andrade[50], M. Antonello[50], S. Bollweg[50], M. Bonanomi[50], K. El Morabit[50], Y. Fischer[50], M. Frahm[50], E. Garutti[50], A. Grohsjean[50], A.A. Guvenli[50], J. Haller[50], D. Hundhausen[50], G. Kasieczka[50], P. Keicher[50], R. Klanner[50], W. Korcari[50], T. Kramer[50], C.c. Kuo[50], F. Labe[50], J. Lange[50], A. Lobanov[50], L. Moureaux[50], A. Nigamova[50], K. Nikolopoulos[50], A. Paasch[50], K.J. Pena Rodriguez[50], N. Prouvost[50], B. Raciti[50], M. Rieger[50], D. Savoiu[50], P. Schleper[50], M. Schröder[50], J. Schwandt[50], M. Sommerhalder[50], H. Stadie[50], G. Steinbrück[50], R. Ward[50], B. Wiederspan[50], M. Wolf[50], S. Brommer[51], E. Butz[51], Y.M. Chen[51], T. Chwalek[51], A. Dierlamm[51], G.G. Dincer[51], U. Elicabuk[51], N. Faltermann[51], M. Giffels[51], A. Gottmann[51], F. Hartmann[51,ac], M. Horzela[51], F. Hummer[51], U. Husemann[51], J. Kieseler[51], M. Klute[51], R. Kunnilan Muhammed Rafeek[51], O. Lavoryk[51], J.M. Lawhorn[51], A. Lintuluoto[51], S. Maier[51], M. Mormile[51], Th. Müller[51], E. Pfeffer[51], M. Presilla[51], G. Quast[51], K. Rabbertz[51], B. Regnery[51], R. Schmieder[51], N. Shadskiy[51], I. Shvetsov[51], H.J. Simonis[51], L. Sowa[51], L. Stockmeier[51], K. Tauqeer[51], M. Toms[51], B. Topko[51], N. Trevisani[51], C. Verstege[51], T. Voigtländer[51], R.F. Von Cube[51], J. Von Den Driesch[51], M. Wassmer[51], R. Wolf[51], W.D. Zeuner[51], X. Zuo[51], G. Anagnostou[52], G. Daskalakis[52], A. Kyriakis[52], G. Melachroinos[53], Z. Painesis[53], I. Paraskevas[53], N. Saoulidou[53], K. Theofilatos[53], E. Tziaferi[53], E. Tzovara[53], K. Vellidis[53], I. Zisopoulos[53], T. Chatzistavrou[54], G. Karapostoli[54], K. Kousouris[54], E. Siamarkou[54], G. Tsipolitis[54], I. Bestintzanos[55], I. Evangelou[55], C. Foudas[55], P. Katsoulis[55], P. Kokkas[55], P.G. Kosmoglou Kioseoglou[55], N. Manthos[55], I. Papadopoulos[55], J. Strologas[55], D. Druzhkin[56], C. Hajdu[56], D. Horvath[56,ad,ae], K. Márton[56], A.J. Rádl[56,af], F. Sikler[56], V. Veszpremi[56], M. Csanád[57], K. Farkas[57], A. Fehérkuti[57,ag], M.M.A. Gadallah[57,ah], Á. Kadlecsik[57], M. León Coello[57], G. Pásztor[57], G.I. Veres[57], B. Ujvari[58], G. Zilizi[58], G. Bencze[59], S. Czellar[59], J. Molnar[59], Z. Szillasi[59], T. Csorgo[60,ag], F. Nemes[60,ag], T. Novak[60], I. Szanyi[60,ai], S. Bansal[61], S.B. Beri[61], V. Bhatnagar[61], G. Chaudhary[61], S. Chauhan[61], N. Dhingra[61,aj], A. Kaur[61], A. Kaur[61], H. Kaur[61], M. Kaur[61], S. Kumar[61], T. Sheokand[61], J.B. Singh[61], A. Singla[61], A. Bhardwaj[62], A. Chhetri[62], B.C. Choudhary[62], A. Kumar[62], A. Kumar[62], M. Naimuddin[62], S. Phor[62], K. Ranjan[62], M.K. Saini[62], P. Palni[63], S. Acharya[64,ak], B. Gomber[64], S. Mukherjee[65], S. Bhattacharya[66], S. Das Gupta[66], S. Dutta[66], S. Dutta[66], S. Sarkar[66], M.M. Ameen[67], P.K. Behera[67], S. Chatterjee[67], G. Dash[67], A. Dattamunsi[67], P. Jana[67], P. Kalbhor[67], S. Kamble[67], J.R. Komaragiri[67,al], T. Mishra[67], P.R. Pujahari[67], A.K. Sikdar[67], R.K. Singh[67], P. Verma[67], S. Verma[67], A. Vijay[67], B.K. Sirasva[68], L. Bhatt[69], S. Dugad[69], G.B. Mohanty[69], M. Shelake[69], P. Suryadevara[69], A. Bala[70], S. Banerjee[70], S. Barman[70,am], R.M. Chatterjee[70], M. Guchait[70], Sh. Jain[70], A. Jaiswal[70], B.M. Joshi[70], S. Kumar[70], M. Maity[70,am], G. Majumder[70], K. Mazumdar[70], S. Parolia[70], R. Saxena[70], A. Thachayath[70], S. Bahinipati[71,an], D. Maity[71,ao], P. Mal[71], K. Naskar[71,ao], A. Nayak[71,ao], S. Nayak[71], K. Pal[71], R. Raturi[71], P. Sadangi[71], S.K. Swain[71], S. Varghese[71,ao], D. Vats[71,ao], A. Alpana[72], S. Dube[72], P. Hazarika[72], B. Kansal[72],

JHEP07(2026)119

A. Laha[72], R. Sharma[72], S. Sharma[72], K.Y. Vaish[72], S. Ghosh[73], H. Bakhshiansohi[74,ap], A. Jafari[74,aq], V. Sedighzadeh Dalavi[74], M. Zeinali[74,ar], S. Bashiri[75], S. Chenarani[75,as], S.M. Etesami[75], Y. Hosseini[75], M. Khakzad[75], E. Khazaie[75], M. Mohammadi Najafabadi[75], S. Tizchang[75,at], M. Felcini[76], M. Grunewald[76], M. Abbrescia[77a,77b], M. Barbieri[77a,77b], M. Buonsante[77a,77b], A. Colaleo[77a,77b], D. Creanza[77a,77c], N. De Filippis[77a,77c], M. De Palma[77a,77b], W. Elmetenawee[77a,77b,au], N. Ferrara[77a,77c], L. Fiore[77a], L. Longo[77a], M. Louka[77a,77b], G. Maggi[77a,77c], M. Maggi[77a], I. Margjeka[77a], V. Mastrapasqua[77a,77b], S. My[77a,77b], F. Nenna[77a,77b], S. Nuzzo[77a,77b], A. Pellecchia[77a,77b], A. Pompili[77a,77b], G. Pugliese[77a,77c], R. Radogna[77a,77b], D. Ramos[77a], A. Ranieri[77a], L. Silvestris[77a], F.M. Simone[77a,77c], Ü. Sözbilir[77a], A. Stamerra[77a,77b], D. Troiano[77a,77b], R. Venditti[77a,77b], P. Verwilligen[77a], A. Zaza[77a,77b], G. Abbiendi[78a], D. Bonacorsi[78a,78b], P. Capiluppi[78a,78b], M. Cuffiani[78a,78b], G.M. Dallavalle[78a], T. Diotalevi[78a,78b], F. Fabbri[78a], A. Fanfani[78a,78b], R. Farinelli[78a], D. Fasanella[78a], P. Giacomelli[78a], C. Grandi[78a], L. Guiducci[78a,78b], S. Lo Meo[78a,av], M. Lorusso[78a,78b], L. Lunerti[78a], S. Marcellini[78a], G. Masetti[78a], F.L. Navarria[78a,78b], G. Paggi[78a,78b], A. Perrotta[78a], F. Primavera[78a,78b], A.M. Rossi[78a,78b], S. Rossi Tisbeni[78a,78b], T. Rovelli[78a,78b], G.P. Siroli[78a,78b], S. Costa[79a,79b,aw], A. Di Mattia[79a], A. Lapertosa[79a], R. Potenza[79a,79b], A. Tricomi[79a,79b,aw], J. Altork[80a,80b], P. Assiouras[80a], G. Barbagli[80a], G. Bardelli[80a], M. Bartolini[80a,80b], A. Calandri[80a,80b], B. Camaiani[80a,80b], A. Cassese[80a], R. Ceccarelli[80a], V. Ciulli[80a,80b], C. Civinini[80a], R. D'Alessandro[80a,80b], L. Damenti[80a,80b], E. Focardi[80a,80b], T. Kello[80a], G. Latino[80a,80b], P. Lenzi[80a,80b], M. Lizzo[80a], M. Meschini[80a], S. Paoletti[80a], A. Papanastassiou[80a,80b], G. Sguazzoni[80a], L. Viliani[80a], L. Benussi[81], S. Bianco[81], S. Meola[81,ax], D. Piccolo[81], M. Alves Gallo Pereira[82a], F. Ferro[82a], E. Robutti[82a], S. Tosi[82a,82b], A. Benaglia[83a], F. Brivio[83a], V. Camagni[83a,83b], F. Cetorelli[83a,83b], F. De Guio[83a,83b], M.E. Dinardo[83a,83b], P. Dini[83a], S. Gennai[83a], R. Gerosa[83a,83b], A. Ghezzi[83a,83b], P. Govoni[83a,83b], L. Guzzi[83a], M.R. Kim[83a], G. Lavizzari[83a,83b], M.T. Lucchini[83a,83b], M. Malberti[83a], S. Malvezzi[83a], A. Massironi[83a], D. Menasce[83a], L. Moroni[83a], M. Paganoni[83a,83b], S. Palluotto[83a,83b], D. Pedrini[83a], A. Perego[83a,83b], G. Pizzati[83a,83b], T. Tabarelli de Fatis[83a,83b], S. Buontempo[84a], C. Di Fraia[84a,84b], F. Fabozzi[84a,84c], L. Favilla[84a,84d], A.O.M. Iorio[84a,84b], L. Lista[84a,84b,ay], P. Paolucci[84a,ac], B. Rossi[84a], P. Azzi[85a], N. Bacchetta[85a,az], D. Bisello[85a,85b], P. Bortignon[85a,85c], G. Bortolato[85a,85b], A.C.M. Bulla[85a,85c], R. Carlin[85a,85b], T. Dorigo[85a,ba], F. Fanzago[85a], F. Gasparini[85a,85b], S. Giorgetti[85a], E. Lusiani[85a], M. Margoni[85a,85b], A.T. Meneguzzo[85a,85b], J. Pazzini[85a,85b], P. Ronchese[85a,85b], R. Rossin[85a,85b], F. Simonetto[85a,85b], M. Tosi[85a,85b], A. Triossi[85a,85b], S. Ventura[85a], M. Zanetti[85a,85b], P. Zotto[85a,85b], A. Zucchetta[85a,85b], G. Zumerle[85a,85b], A. Braghieri[86a], S. Calzaferri[86a], P. Montagna[86a,86b], M. Pelliccioni[86a], V. Re[86a], C. Riccardi[86a,86b], P. Salvini[86a], I. Vai[86a,86b], P. Vitulo[86a,86b], S. Ajmal[87a,87b], M.E. Ascioti[87a,87b], G.M. Bilei[87a,†], C. Carrivale[87a,87b], D. Ciangottini[87a,87b], L. Della Penna[87a,87b], L. Fanò[87a,87b], V. Mariani[87a,87b], M. Menichelli[87a], F. Moscatelli[87a,bb], A. Rossi[87a,87b], A. Santocchia[87a,87b], D. Spiga[87a], T. Tedeschi[87a,87b], C. Aimè[88a,88b], C.A. Alexe[88a,88c], P. Asenov[88a,88b], P. Azzurri[88a], G. Bagliesi[88a], L. Bianchini[88a,88b], T. Boccali[88a], E. Bossini[88a], D. Bruschini[88a,88c], L. Calligaris[88a,88b], R. Castaldi[88a], F. Cattafesta[88a,88c], M.A. Ciocci[88a,88d], M. Cipriani[88a,88b], R. Dell'Orso[88a], S. Donato[88a,88b], R. Forti[88a,88b], A. Giassi[88a], F. Ligabue[88a,88c], A.C. Marini[88a,88b], D. Matos Figueiredo[88a], A. Messineo[88a,88b], S. Mishra[88a], V.K. Muraleedharan Nair Bindhu[88a,88b], S. Nandan[88a], F. Palla[88a], M. Riggirello[88a,88c], A. Rizzi[88a,88b], G. Rolandi[88a,88c], S. Roy Chowdhury[88a,bc], T. Sarkar[88a], A. Scribano[88a], P. Solanki[88a,88b], P. Spagnolo[88a], F. Tenchini[88a,88b], R. Tenchini[88a], G. Tonelli[88a,88b], N. Turini[88a,88d], F. Vaselli[88a,88c], A. Venturi[88a], P.G. Verdini[88a], P. Akrap[89a,89b], C. Basile[89a,89b], S.C. Behera[89a], F. Cavallari[89a], L. Cunqueiro Mendez[89a,89b], F. De Riggi[89a,89b], D. Del Re[89a,89b], E. Di Marco[89a], M. Diemoz[89a], F. Errico[89a], L. Frosina[89a,89b], R. Gargiulo[89a,89b], B. Harikrishnan[89a,89b], F. Lombardi[89a,89b], E. Longo[89a,89b], L. Martikainen[89a,89b], J. Mijuskovic[89a,89b], G. Organtini[89a,89b], N. Palmeri[89a,89b], R. Paramatti[89a,89b], S. Rahatlou[89a,89b], C. Rovelli[89a], F. Santanastasio[89a,89b], L. Soffi[89a], V. Vladimirov[89a,89b], N. Amapane[90a,90b], R. Arcidiacono[90a,90c], S. Argiro[90a,90b], M. Arneodo[90a,90c], N. Bartosik[90a,90c], R. Bellan[90a,90b], A. Bellora[90a,90b], C. Biino[90a], C. Borca[90a,90b], N. Cartiglia[90a], M. Costa[90a,90b], R. Covarelli[90a,90b], N. Demaria[90a], L. Finco[90a], M. Grippo[90a,90b], B. Kiani[90a,90b], L. Lanteri[90a,90b], F. Legger[90a], F. Luongo[90a,90b], C. Mariotti[90a], S. Maselli[90a], A. Mecca[90a,90b], L. Menzio[90a,90b], P. Meridiani[90a], E. Migliore[90a,90b], M. Monteno[90a], M.M. Obertino[90a,90b], G. Ortona[90a], L. Pacher[90a,90b], N. Pastrone[90a], M. Ruspa[90a,90c], F. Siviero[90a,90b], V. Sola[90a,90b], A. Solano[90a,90b], A. Staiano[90a], C. Tarricone[90a,90b], D. Trocino[90a], G. Umoret[90a,90b], E. Vlasov[90a,90b], R. White[90a,90b], J. Babbar[91a,91b], S. Belforte[91a], V. Candelise[91a,91b], M. Casarsa[91a], F. Cossutti[91a], K. De Leo[91a], G. Della Ricca[91a,91b], R. Delli Gatti[91a,91b], S. Dogra[92], J. Hong[92], J. Kim[92], T. Kim[92], D. Lee[92], H. Lee[92], J. Lee[92], S.W. Lee[92], C.S. Moon[92], Y.D. Oh[92], S. Sekmen[92], B. Tae[92], Y.C. Yang[92], M.S. Kim[93], G. Bak[94], P. Gwak[94], H. Kim[94], D.H. Moon[94], J. Seo[94], E. Asilar[95], F. Carnevali[95], J. Choi[95,bd], T.J. Kim[95], Y. Ryou[95], S. Ha[96], S. Han[96], B. Hong[96], J. Kim[96], K. Lee[96], K.S. Lee[96], S. Lee[96], J. Yoo[96], J. Goh[97], J. Shin[97], S. Yang[97], Y. Kang[98], H. S. Kim[98], Y. Kim[98], S. Lee[98], J. Almond[99], J.H. Bhyun[99], J. Choi[99], J. Choi[99], W. Jun[99], H. Kim[99], J. Kim[99], T. Kim[99], Y. Kim[99], Y.W. Kim[99], S. Ko[99], H. Lee[99], J. Lee[99], J. Lee[99], B.H. Oh[99], S.B. Oh[99], J. Shin[99], U.K. Yang[99], I. Yoon[99], W. Jang[100], D.Y. Kang[100], D. Kim[100], S. Kim[100], B. Ko[100], J.S.H. Lee[100], Y. Lee[100], I.C. Park[100], Y. Roh[100], I.J. Watson[100], G. Cho[101], K. Hwang[101], B. Kim[101], S. Kim[101], K. Lee[101], H.D. Yoo[101], Y. Lee[102], I. Yu[102], T. Beyrouthy[103], Y. Gharbia[103], F. Alazemi[104], K. Dreimanis[105], O.M. Eberlins[105], A. Gaile[105], C. Munoz Diaz[105], D. Osite[105], G. Pikurs[105], R. Plese[105], A. Potrebko[105], M. Seidel[105], D. Sidiropoulos Kontos[105], N.R. Strautnieks[106], M. Ambrozas[107], A. Juodagalvis[107], S. Nargelas[107], A. Rinkevicius[107], G. Tamulaitis[107], I. Yusuff[108,be], Z. Zolkapli[108], J.F. Benitez[109], A. Castaneda Hernandez[109], A. Cota Rodriguez[109], L.E. Cuevas Picos[109], H.A. Encinas Acosta[109], L.G. Gallegos Maríñez[109], J.A. Murillo Quijada[109], L. Valencia Palomo[109], G. Ayala[110], H. Castilla-Valdez[110], H. Crotte Ledesma[110], R. Lopez-Fernandez[110], J. Mejia Guisao[110], R. Reyes-Almanza[110], A. Sánchez Hernández[110], C. Oropeza Barrera[111], M. Ramírez García[111], D.L. Ramirez Guadarrama[111], I. Bautista[112], F.E. Neri Huerta[112], I. Pedraza[112], H.A. Salazar Ibarguen[112], C. Uribe Estrada[112], I. Bubanja[113], N. Raicevic[113], P.H. Butler[114], A. Ahmad[115], M.I. Asghar[115], A. Awais[115], M.I.M. Awan[115], W.A. Khan[115], V. Avati[116], L. Forthomme[116], L. Grzanka[116], M. Malawski[116], K. Piotrzkowski[116], M. Bluj[117], M. Górski[117], M. Kazana[117], M. Szleper[117], P. Zalewski[117], K. Bunkowski[118], K. Doroba[118], A. Kalinowski[118], M. Konecki[118], J. Krolikowski[118], A. Muhammad[118], P. Fokow[119], K. Pozniak[119], W. Zabolotny[119], M. Araujo[120], D. Bastos[120], C. Beirão Da Cruz E Silva[120], A. Boletti[120], M. Bozzo[120], T. Camporesi[120], G. Da Molin[120], M. Gallinaro[120], J. Hollar[120], N. Leonardo[120], G.B. Marozzo[120], A. Petrilli[120], M. Pisano[120], J. Seixas[120], J. Varela[120], J.W. Wulff[120], P. Adzic[121], L. Markovic[121], P. Milenovic[121], V. Milosevic[121], D. Devetak[122], M. Dordevic[122], J. Milosevic[122], L. Nadderd[122], V. Rekovic[122], M. Stojanovic[122], M. Alcalde Martinez[123], J. Alcaraz Maestre[123], Cristina F. Bedoya[123], J.A. Brochero Cifuentes[123], Oliver M. Carretero[123], M. Cepeda[123], M. Cerrada[123], N. Colino[123], B. De La Cruz[123], A. Delgado Peris[123], A. Escalante Del Valle[123], D. Fernández Del Val[123], J.P. Fernández Ramos[123], J. Flix[123], M.C. Fouz[123], M. Gonzalez Hernandez[123], O. Gonzalez Lopez[123], S. Goy Lopez[123], J.M. Hernandez[123], M.I. Josa[123], J. Llorente Merino[123], C. Martin Perez[123], E. Martin Viscasillas[123], D. Moran[123], C. M. Morcillo Perez[123], Á. Navarro Tobar[123], R. Paz Herrera[123], C. Perez Dengra[123], A. Pérez-Calero Yzquierdo[123], J. Puerta Pelayo[123], I. Redondo[123], J. Vazquez Escobar[123], J.F. de Trocóniz[124], B. Alvarez Gonzalez[125], J. Ayllon Torresano[125], A. Cardini[125], J. Cuevas[125], J. Del Riego Badas[125], D. Estrada Acevedo[125], J. Fernandez Menendez[125], S. Folgueras[125], I. Gonzalez Caballero[125], P. Leguina[125], M. Obeso Menendez[125], E. Palencia Cortezon[125], J. Prado Pico[125], A. Soto Rodríguez[125], C. Vico Villalba[125], P. Vischia[125], S. Blanco Fernández[126], I.J. Cabrillo[126], A. Calderon[126], J. Duarte Campderros[126], M. Fernandez[126], G. Gomez[126], C. Lasaosa García[126], R. Lopez Ruiz[126], C. Martinez Rivero[126], P. Martinez Ruiz del Arbol[126], F. Matorras[126], P. Matorras Cuevas[126], E. Navarrete Ramos[126], J. Piedra Gomez[126], C. Quintana San Emeterio[126], L. Scodellaro[126], I. Vila[126], R. Vilar Cortabitarte[126], J.M. Vizan Garcia[126], B. Kailasapathy[127,bf], D.D.C. Wickramarathna[127], W.G.D. Dharmaratna[128,bg], K. Liyanage[128], N. Perera[128], D. Abbaneo[129], C. Amendola[129], R. Ardino[129], E. Auffray[129], J. Baechler[129], D. Barney[129], J. Bendavid[129], M. Bianco[129], A. Bocci[129], L. Borgonovi[129], C. Botta[129], A. Bragagnolo[129], C.E. Brown[129], C. Caillol[129], G. Cerminara[129], P. Connor[129], D. d'Enterria[129], A. Dabrowski[129], A. David[129], A. De Roeck[129], M.M. Defranchis[129], M. Deile[129], M. Dobson[129], P.J. Fernández Manteca[129], B.A. Fontana Santos Alves[129], E. Fontanesi[129], W. Funk[129], A. Gaddi[129], S. Giani[129], D. Gigi[129], K. Gill[129], F. Glege[129], M. Glowacki[129], A. Gruber[129], J. Hegeman[129], J.K. Heikkilä[129], R. Hofsaess[129], B. Huber[129], T. James[129], P. Janot[129], O. Kaluzinska[129], O. Karacheban[129,z], G. Karathanasis[129], S. Laurila[129], P. Lecoq[129], E. Leutgeb[129], C. Lourenço[129], A.-M. Lyon[129], M. Magherini[129], L. Malgeri[129], M. Mannelli[129], A. Mehta[129], F. Meijers[129], J.A. Merlin[129], S. Mersi[129], E. Meschi[129], M. Migliorini[129], F. Monti[129], F. Moortgat[129], M. Mulders[129], M. Musich[129], I. Neutelings[129], S. Orfanelli[129], F. Pantaleo[129], M. Pari[129], G. Petrucciani[129], A. Pfeiffer[129], M. Pierini[129], M. Pitt[129], H. Qu[129], D. Rabady[129], A. Reimers[129], B. Ribeiro Lopes[129], F. Riti[129], P. Rosado[129], M. Rovere[129], H. Sakulin[129],

R. Salvatico[129], S. Sanchez Cruz[129], S. Scarfi[129], M. Selvaggi[129], A. Sharma[129], K. Shchelina[129], P. Silva[129], P. Sphicas[129,bh], A.G. Stahl Leiton[129], A. Steen[129], S. Summers[129], D. Treille[129], P. Tropea[129], E. Vernazza[129], J. Wanczyk[129,bi], S. Wuchterl[129], M. Zarucki[129], P. Zehetner[129], P. Zejdl[129], G. Zevi Della Porta[129], T. Bevilacqua[130,bj], L. Caminada[130,bj], W. Erdmann[130], R. Horisberger[130], Q. Ingram[130], H.C. Kaestli[130], D. Kotlinski[130], C. Lange[130], U. Langenegger[130], L. Noehte[130,bj], T. Rohe[130], A. Samalan[130], T.K. Aarrestad[131], M. Backhaus[131], G. Bonomelli[131], C. Cazzaniga[131], K. Datta[131], P. De Bryas Dexmiers D'Archiacchiac[131,bi], A. De Cosa[131], G. Dissertori[131], M. Dittmar[131], M. Donegà[131], F. Eble[131], K. Gedia[131], F. Glessgen[131], C. Grab[131], N. Härringer[131], T.G. Harte[131], W. Lustermann[131], M. Malucchi[131], R.A. Manzoni[131], L. Marchese[131], A. Mascellani[131,bi], F. Nessi-Tedaldi[131], F. Pauss[131], V. Perovic[131], B. Ristic[131], R. Seidita[131], J. Steggemann[131,bi], A. Tarabini[131], D. Valsecchi[131], R. Wallny[131], C. Amsler[132,bk], P. Bärtschi[132], F. Bilandzija[132], M.F. Canelli[132], G. Celotto[132], K. Cormier[132], M. Huwiler[132], W. Jin[132], A. Jofrehei[132], B. Kilminster[132], T.H. Kwok[132], S. Leontsinis[132], V. Lukashenko[132], A. Macchiolo[132], F. Meng[132], M. Missiroli[132], J. Motta[132], P. Robmann[132], M. Senger[132], E. Shokr[132], F. Stäger[132], R. Tramontano[132], P. Viscone[132], D. Bhowmik[133], C.M. Kuo[133], P.K. Rout[133], S. Taj[133], P.C. Tiwari[133,al], L. Ceard[134], K.F. Chen[134], Z.g. Chen[134], A. De Iorio[134], W.-S. Hou[134], T.h. Hsu[134], Y.w. Kao[134], S. Karmakar[134], G. Kole[134], Y.y. Li[134], R.-S. Lu[134], E. Paganis[134], X.f. Su[134], J. Thomas-Wilsker[134], L.s. Tsai[134], D. Tsionou[134], H.y. Wu[134], E. Yazgan[134], C. Asawatangtrakuldee[135], N. Srimanobhas[135], Y. Maghrbi[136], D. Agyel[137], F. Dolek[137], I. Dumanoglu[137,bl], Y. Guler[137,bm], E. Gurpinar Guler[137,bm], C. Isik[137], O. Kara[137], A. Kayis Topaksu[137], Y. Komurcu[137], G. Onengut[137], K. Ozdemir[137,bn], B. Tali[137,bo], U.G. Tok[137], E. Uslan[137], I.S. Zorbakir[137], S. Sen[138], M. Yalvac[139,bp], B. Akgun[140], I.O. Atakisi[140,bq], E. Gülmez[140], M. Kaya[140,br], O. Kaya[140,bs], M.A. Sarkisla[140,bt], S. Tekten[140,bu], D. Boncukcu[141], A. Cakir[141], K. Cankocak[141,bl,bv], B. Hacisahinoglu[142], I. Hos[142,bw], B. Kaynak[142], S. Ozkorucuklu[142], O. Potok[142], H. Sert[142], C. Simsek[142], C. Zorbilmez[142], S. Cerci[143], C. Dozen[143,bx], B. Isildak[143,by], E. Simsek[143], D. Sunar Cerci[143], T. Yetkin[143,bx], A. Boyaryntsev[144], O. Dadazhanova[144], B. Grynyov[144], L. Levchuk[145], J.J. Brooke[146], A. Bundock[146], F. Bury[146], E. Clement[146], D. Cussans[146], D. Dharmender[146], H. Flacher[146], J. Goldstein[146], H.F. Heath[146], M.-L. Holmberg[146], L. Kreczko[146], S. Paramesvaran[146], L. Robertshaw[146], M.S. Sanjrani[146,ap], J. Segal[146], V.J. Smith[146], A.H. Ball[147], K.W. Bell[147], A. Belyaev[147,bz], C. Brew[147], R.M. Brown[147], D.J.A. Cockerill[147], A. Elliot[147], K.V. Ellis[147], J. Gajownik[147], K. Harder[147], S. Harper[147], J. Linacre[147], K. Manolopoulos[147], M. Moallemi[147], D.M. Newbold[147], E. Olaiya[147], D. Petyt[147], T. Reis[147], A.R. Sahasransu[147], G. Salvi[147], T. Schuh[147], C.H. Shepherd-Themistocleous[147], I.R. Tomalin[147], K.C. Whalen[147], T. Williams[147], I. Andreou[148], R. Bainbridge[148], P. Bloch[148], O. Buchmuller[148], C.A. Carrillo Montoya[148], D. Colling[148], I. Das[148], P. Dauncey[148], G. Davies[148], M. Della Negra[148], S. Fayer[148], G. Fedi[148], G. Hall[148], H.R. Hoorani[148], A. Howard[148], G. Iles[148], C.R. Knight[148], P. Krueper[148], J. Langford[148], K.H. Law[148], J. León Holgado[148], L. Lyons[148], A.-M. Magnan[148], B. Maier[148], S. Mallios[148], A. Mastronikolis[148], M. Mieskolainen[148], J. Nash[148,ca], M. Pesaresi[148],

JHEP07(2026)119

P.B. Pradeep[148], B.C. Radburn-Smith[148], A. Richards[148], A. Rose[148], L. Russell[148], K. Savva[148], C. Seez[148], R. Shukla[148], A. Tapper[148], K. Uchida[148], G.P. Uttley[148], T. Virdee[148,ac], M. Vojinovic[148], N. Wardle[148], D. Winterbottom[148], J.E. Cole[149], A. Khan[149], P. Kyberd[149], I.D. Reid[149], S. Abdullin[150], A. Brinkerhoff[150], E. Collins[150], M.R. Darwish[150], J. Dittmann[150], K. Hatakeyama[150], V. Hegde[150], J. Hiltbrand[150], B. McMaster[150], J. Samudio[150], S. Sawant[150], C. Sutantawibul[150], J. Wilson[150], J.M. Hogan[151], R. Bartek[152], A. Dominguez[152], S. Raj[152], B. Sahu[152,ak], A.E. Simsek[152], S.S. Yu[152], B. Bam[153], A. Buchot Perraguin[153], S. Campbell[153], R. Chudasama[153], S.I. Cooper[153], C. Crovella[153], G. Fidalgo[153], S.V. Gleyzer[153], A. Khukhunaishvili[153], K. Matchev[153], E. Pearson[153], C.U. Perez[153], P. Rumerio[153,cb], E. Usai[153], R. Yi[153], S. Cholak[154], G. De Castro[154], Z. Demiragli[154], C. Erice[154], C. Fangmeier[154], C. Fernandez Madrazo[154], J. Fulcher[154], F. Golf[154], S. Jeon[154], J. O'Cain[154], I. Reed[154], J. Rohlf[154], K. Salyer[154], D. Sperka[154], D. Spitzbart[154], I. Suarez[154], A. Tsatsos[154], E. Wurtz[154], A.G. Zecchinelli[154], G. Barone[155], G. Benelli[155], D. Cutts[155], S. Ellis[155], L. Gouskos[155], M. Hadley[155], U. Heintz[155], K.W. Ho[155], T. Kwon[155], L. Lambrecht[155], G. Landsberg[155], K.T. Lau[155], J. Luo[155], S. Mondal[155], J. Roloff[155], T. Russell[155], S. Sagir[155,cc], X. Shen[155], M. Stamenkovic[155], N. Venkatasubramanian[155], S. Abbott[156], S. Baradia[156], B. Barton[156], R. Breedon[156], H. Cai[156], M. Calderon De La Barca Sanchez[156], E. Cannaert[156], M. Chertok[156], M. Citron[156], J. Conway[156], P.T. Cox[156], R. Erbacher[156], O. Kukral[156], G. Mocellin[156], S. Ostrom[156], I. Salazar Segovia[156], J.S. Tafoya Vargas[156], W. Wei[156], S. Yoo[156], K. Adamidis[157], M. Bachtis[157], D. Campos[157], R. Cousins[157], A. Datta[157], G. Flores Avila[157], J. Hauser[157], M. Ignatenko[157], M.A. Iqbal[157], T. Lam[157], Y.f. Lo[157], E. Manca[157], A. Nunez Del Prado[157], D. Saltzberg[157], V. Valuev[157], R. Clare[158], J.W. Gary[158], G. Hanson[158], A. Aportela[159], A. Arora[159], J.G. Branson[159], S. Cittolin[159], S. Cooperstein[159], B. D'Anzi[159], D. Diaz[159], J. Duarte[159], L. Giannini[159], Y. Gu[159], J. Guiang[159], V. Krutelyov[159], R. Lee[159], J. Letts[159], H. Li[159], M. Masciovecchio[159], F. Mokhtar[159], S. Mukherjee[159], M. Pieri[159], D. Primosch[159], M. Quinnan[159], V. Sharma[159], M. Tadel[159], E. Vourliotis[159], F. Würthwein[159], A. Yagil[159], Z. Zhao[159], A. Barzdukas[160], L. Brennan[160], C. Campagnari[160], S. Carron Montero[160,cd], K. Downham[160], C. Grieco[160], M.M. Hussain[160], J. Incandela[160], M.W.K. Lai[160], A.J. Li[160], P. Masterson[160], J. Richman[160], S.N. Santpur[160], U. Sarica[160], R. Schmitz[160], F. Setti[160], J. Sheplock[160], D. Stuart[160], T.Á. Vámi[160], X. Yan[160], D. Zhang[160], A. Albert[161], S. Bhattacharya[161], A. Bornheim[161], O. Cerri[161], R. Kansal[161], J. Mao[161], H.B. Newman[161], G. Reales Gutiérrez[161], T. Sievert[161], M. Spiropulu[161], J.R. Vlimant[161], R.A. Wynne[161], S. Xie[161], J. Alison[162], S. An[162], M. Cremonesi[162], V. Dutta[162], E.Y. Ertorer[162], T. Ferguson[162], T.A. Gómez Espinosa[162], A. Harilal[162], A. Kallil Tharayil[162], M. Kanemura[162], C. Liu[162], M. Marchegiani[162], P. Meiring[162], T. Mudholkar[162], S. Murthy[162], P. Palit[162], K. Park[162], M. Paulini[162], A. Roberts[162], A. Sanchez[162], W. Terrill[162], J.P. Cumalat[163], W.T. Ford[163], A. Hart[163], S. Kwan[163], J. Pearkes[163], C. Savard[163], N. Schonbeck[163], K. Stenson[163], K.A. Ulmer[163], S.R. Wagner[163], N. Zipper[163], D. Zuolo[163], J. Alexander[164], X. Chen[164], J. Dickinson[164], A. Duquette[164], J. Fan[164], X. Fan[164], J. Grassi[164], S. Hogan[164], P. Kotamnives[164],

J. Monroy[164], G. Niendorf[164], M. Oshiro[164], J.R. Patterson[164], A. Ryd[164], J. Thom[164], P. Wittich[164], R. Zou[164], L. Zygala[164], M. Albrow[165], M. Alyari[165], O. Amram[165], G. Apollinari[165], A. Apresyan[165], L.A.T. Bauerdick[165], D. Berry[165], J. Berryhill[165], P.C. Bhat[165], K. Burkett[165], J.N. Butler[165], A. Canepa[165], G.B. Cerati[165], H.W.K. Cheung[165], F. Chlebana[165], C. Cosby[165], G. Cummings[165], I. Dutta[165], V.D. Elvira[165], J. Freeman[165], A. Gandrakota[165], Z. Gecse[165], L. Gray[165], D. Green[165], A. Grummer[165], S. Grünendahl[165], D. Guerrero[165], O. Gutsche[165], R.M. Harris[165], T.C. Herwig[165], J. Hirschauer[165], V. Innocente[165], B. Jayatilaka[165], S. Jindariani[165], M. Johnson[165], U. Joshi[165], B. Klima[165], K.H.M. Kwok[165], S. Lammel[165], C. Lee[165], D. Lincoln[165], R. Lipton[165], T. Liu[165], K. Maeshima[165], D. Mason[165], P. McBride[165], P. Merkel[165], S. Mrenna[165], S. Nahn[165], J. Ngadiuba[165], D. Noonan[165], S. Norberg[165], V. Papadimitriou[165], N. Pastika[165], K. Pedro[165], C. Pena[165,ce], C.E. Perez Lara[165], F. Ravera[165], A. Reinsvold Hall[165,cf], L. Ristori[165], M. Safdari[165], E. Sexton-Kennedy[165], N. Smith[165], A. Soha[165], L. Spiegel[165], S. Stoynev[165], J. Strait[165], L. Taylor[165], S. Tkaczyk[165], N.V. Tran[165], L. Uplegger[165], E.W. Vaandering[165], C. Wang[165], I. Zoi[165], C. Aruta[166], P. Avery[166], D. Bourilkov[166], P. Chang[166], V. Cherepanov[166], R.D. Field[166], C. Huh[166], E. Koenig[166], M. Kolosova[166], J. Konigsberg[166], A. Korytov[166], G. Mitselmakher[166], K. Mohrman[166], A. Muthirakalayil Madhu[166], N. Rawal[166], S. Rosenzweig[166], V. Sulimov[166], Y. Takahashi[166], J. Wang[166], T. Adams[167], A. Al Kadhim[167], A. Askew[167], S. Bower[167], R. Goff[167], R. Hashmi[167], A. Hassani[167], R.S. Kim[167], T. Kolberg[167], G. Martinez[167], M. Mazza[167], H. Prosper[167], P.R. Prova[167], R. Yohay[167], B. Alsufyani[168], S. Butalla[168], S. Das[168], M. Hohlmann[168], M. Lavinsky[168], E. Yanes[168], M.R. Adams[169], N. Barnett[169], A. Baty[169], C. Bennett[169], R. Cavanaugh[169], R. Escobar Franco[169], O. Evdokimov[169], C.E. Gerber[169], H. Gupta[169], M. Hawksworth[169], A. Hingrajiya[169], D.J. Hofman[169], Z. Huang[169], J.h. Lee[169], C. Mills[169], S. Nanda[169], G. Nigmatkulov[169], B. Ozek[169], T. Phan[169], D. Pilipovic[169], R. Pradhan[169], E. Prifti[169], P. Roy[169], T. Roy[169], N. Singh[169], M.B. Tonjes[169], N. Varelas[169], M.A. Wadud[169], J. Yoo[169], M. Alhusseini[170], D. Blend[170], K. Dilsiz[170,cg], O.K. Köseyan[170], A. Mestvirishvili[170,ch], O. Neogi[170], H. Ogul[170,ci], Y. Onel[170], A. Penzo[170], C. Snyder[170], E. Tiras[170,cj], B. Blumenfeld[171], J. Davis[171], A.V. Gritsan[171], L. Kang[171], S. Kyriacou[171], P. Maksimovic[171], M. Roguljic[171], S. Sekhar[171], M.V. Srivastav[171], M. Swartz[171], A. Abreu[172], L.F. Alcerro Alcerro[172], J. Anguiano[172], S. Arteaga Escatel[172], P. Baringer[172], A. Bean[172], R. Bhattacharya[172], Z. Flowers[172], D. Grove[172], J. King[172], G. Krintiras[172], M. Lazarovits[172], C. Le Mahieu[172], J. Marquez[172], M. Murray[172], M. Nickel[172], S. Popescu[172,ck], C. Rogan[172], C. Royon[172], S. Rudrabhatla[172], S. Sanders[172], C. Smith[172], G. Wilson[172], B. Allmond[173], N. Islam[173], A. Ivanov[173], K. Kaadze[173], Y. Maravin[173], J. Natoli[173], G.G. Reddy[173], D. Roy[173], G. Sorrentino[173], A. Baden[174], A. Belloni[174], J. Bistany-riebman[174], S.C. Eno[174], N.J. Hadley[174], S. Jabeen[174], R.G. Kellogg[174], T. Koeth[174], B. Kronheim[174], S. Lascio[174], P. Major[174], A.C. Mignerey[174], C. Palmer[174], C. Papageorgakis[174], M.M. Paranjpe[174], E. Popova[174,cl], A. Shevelev[174], L. Zhang[174], C. Baldenegro Barrera[175], H. Bossi[175], S. Bright-Thonney[175], I.A. Cali[175], Y.c. Chen[175], P.c. Chou[175], M. D'Alfonso[175], J. Eysermans[175], C. Freer[175], G. Gomez-Ceballos[175], M. Goncharov[175], G. Grosso[175], P. Harris[175], D. Hoang[175], G.M. Innocenti[175], K. Ivanov[175], D. Kovalskyi[175], J. Krupa[175], L. Lavezzo[175], Y.-J. Lee[175], K. Long[175], C. Mcginn[175], A. Novak[175], M.I. Park[175], C. Paus[175], C. Reissel[175], C. Roland[175], G. Roland[175], S. Rothman[175], T.a. Sheng[175], G.S.F. Stephans[175], D. Walter[175], J. Wang[175], Z. Wang[175], B. Wyslouch[175], T. J. Yang[175], B. Crossman[176], W.J. Jackson[176], C. Kapsiak[176], M. Krohn[176], D. Mahon[176], J. Mans[176], B. Marzocchi[176], R. Rusack[176], O. Sancar[176], R. Saradhy[176], N. Strobbe[176], K. Bloom[177], D.R. Claes[177], G. Haza[177], J. Hossain[177], C. Joo[177], I. Kravchenko[177], A. Rohilla[177], J.E. Siado[177], W. Tabb[177], A. Vagnerini[177], A. Wightman[177], F. Yan[177], H. Bandyopadhyay[178], L. Hay[178], H.w. Hsia[178], I. Iashvili[178], A. Kalogeropoulos[178], A. Kharchilava[178], A. Mandal[178], M. Morris[178], D. Nguyen[178], S. Rappoccio[178], H. Rejeb Sfar[178], A. Williams[178], P. Young[178], D. Yu[178], G. Alverson[179], E. Barberis[179], J. Bonilla[179], B. Bylsma[179], M. Campana[179], J. Dervan[179], Y. Haddad[179], Y. Han[179], I. Israr[179], A. Krishna[179], M. Lu[179], N. Manganelli[179], R. Mccarthy[179], D.M. Morse[179], T. Orimoto[179], L. Skinnari[179], C.S. Thoreson[179], E. Tsai[179], D. Wood[179], S. Dittmer[180], K.A. Hahn[180], M. Mcginnis[180], Y. Miao[180], D.G. Monk[180], M.H. Schmitt[180], A. Taliercio[180], M. Velasco[180], J. Wang[180], G. Agarwal[181], R. Band[181], R. Bucci[181], S. Castells[181], A. Das[181], A. Ehnis[181], R. Goldouzian[181], M. Hildreth[181], K. Hurtado Anampa[181], T. Ivanov[181], C. Jessop[181], A. Karneyeu[181], K. Lannon[181], J. Lawrence[181], N. Loukas[181], L. Lutton[181], J. Mariano[181], N. Marinelli[181], I. Mcalister[181], T. McCauley[181], C. Mcgrady[181], C. Moore[181], Y. Musienko[181,cm], H. Nelson[181], M. Osherson[181], A. Piccinelli[181], R. Ruchti[181], A. Townsend[181], Y. Wan[181], M. Wayne[181], H. Yockey[181], A. Basnet[182], M. Carrigan[182], R. De Los Santos[182], L.S. Durkin[182], C. Hill[182], M. Joyce[182], M. Nunez Ornelas[182], D.A. Wenzl[182], B.L. Winer[182], B. R. Yates[182], H. Bouchamaoui[183], G. Dezoort[183], P. Elmer[183], A. Frankenthal[183], M. Galli[183], B. Greenberg[183], N. Haubrich[183], K. Kennedy[183], G. Kopp[183], Y. Lai[183], D. Lange[183], A. Loeliger[183], D. Marlow[183], I. Ojalvo[183], J. Olsen[183], F. Simpson[183], D. Stickland[183], C. Tully[183], S. Malik[184], R. Sharma[184], S. Chandra[185], R. Chawla[185], A. Gu[185], L. Gutay[185], M. Jones[185], A.W. Jung[185], D. Kondratyev[185], M. Liu[185], G. Negro[185], N. Neumeister[185], G. Paspalaki[185], S. Piperov[185], N.R. Saha[185], J.F. Schulte[185], F. Wang[185], A. Wildridge[185], W. Xie[185], Y. Yao[185], Y. Zhong[185], N. Parashar[186], A. Pathak[186], E. Shumka[186], D. Acosta[187], A. Agrawal[187], C. Arbour[187], T. Carnahan[187], P. Das[187], K.M. Ecklund[187], S. Freed[187], F.J.M. Geurts[187], T. Huang[187], I. Krommydas[187], N. Lewis[187], W. Li[187], J. Lin[187], O. Miguel Colin[187], B.P. Padley[187], R. Redjimi[187], J. Rotter[187], M. Wulansatiti[187], E. Yigitbasi[187], Y. Zhang[187], O. Bessidskaia Bylund[188], A. Bodek[188], P. de Barbaro[188,†], R. Demina[188], A. Garcia-Bellido[188], H.S. Hare[188], O. Hindrichs[188], N. Parmar[188], P. Parygin[188,cl], H. Seo[188], R. Taus[188], B. Chiarito[189], J.P. Chou[189], S.V. Clark[189], S. Donnelly[189], D. Gadkari[189], Y. Gershtein[189], E. Halkiadakis[189], C. Houghton[189], D. Jaroslawski[189], A. Kobert[189], S. Konstantinou[189], I. Laflotte[189], A. Lath[189], J. Martins[189], M. Perez Prada[189], B. Rand[189], J. Reichert[189], P. Saha[189], S. Salur[189], S. Schnetzer[189], S. Somalwar[189], R. Stone[189], S.A. Thayil[189], S. Thomas[189], J. Vora[189], D. Ally[190], A.G. Delannoy[190], S. Fiorendi[190], J. Harris[190], T. Holmes[190], A.R. Kanuganti[190], N. Karunarathna[190], J. Lawless[190], L. Lee[190], E. Nibigira[190], B. Skipworth[190], S. Spanier[190],

JHEP07(2026)119

D. Aebi[191], M. Ahmad[191], T. Akhter[191], K. Androsov[191], A. Bolshov[191], O. Bouhali[191,cn], A. Cagnotta[191], V. D'Amante[191], R. Eusebi[191], P. Flanagan[191], J. Gilmore[191], Y. Guo[191], T. Kamon[191], S. Luo[191], R. Mueller[191], A. Safonov[191], N. Akchurin[192], J. Damgov[192], Y. Feng[192], N. Gogate[192], Y. Kazhykarim[192], K. Lamichhane[192], S.W. Lee[192], C. Madrid[192], A. Mankel[192], T. Peltola[192], I. Volobouev[192], E. Appelt[193], Y. Chen[193], S. Greene[193], A. Gurrola[193], W. Johns[193], R. Kunnawalkam Elayavalli[193], A. Melo[193], D. Rathjens[193], F. Romeo[193], P. Sheldon[193], S. Tuo[193], J. Velkovska[193], J. Viinikainen[193], J. Zhang[193], B. Cardwell[194], H. Chung[194], B. Cox[194], J. Hakala[194], G. Hamilton Ilha Machado[194], R. Hirosky[194], M. Jose[194], A. Ledovskoy[194], C. Mantilla[194], C. Neu[194], C. Ramón Álvarez[194], Z. Wu[194], S. Bhattacharya[195], P.E. Karchin[195], A. Aravind[196], S. Banerjee[196], K. Black[196], T. Bose[196], E. Chavez[196], S. Dasu[196], P. Everaerts[196], C. Galloni[196], H. He[196], M. Herndon[196], A. Herve[196], C.K. Koraka[196], S. Lomte[196], R. Loveless[196], A. Mallampalli[196], A. Mohammadi[196], S. Mondal[196], T. Nelson[196], G. Parida[196], L. Pétré[196], D. Pinna[196], A. Savin[196], V. Shang[196], V. Sharma[196], W.H. Smith[196], D. Teague[196], H.F. Tsoi[196], W. Vetens[196], A. Warden[196], S. Afanasiev[197], V. Alexakhin[197], Yu. Andreev[197], T. Aushev[197], D. Budkouski[197], R. Chistov[197], M. Danilov[197], T. Dimova[197], A. Ershov[197], S. Gninenko[197], I. Gorbunov[197], A. Gribushin[197], A. Kamenev[197], V. Karjavine[197], M. Kirsanov[197], V. Klyukhin[197], O. Kodolova[197,co], V. Korenkov[197], I. Korsakov[197], A. Kozyrev[197], N. Krasnikov[197], A. Lanev[197], A. Malakhov[197], V. Matveev[197], A. Nikitenko[197,cp,cq], V. Palichik[197], V. Perelygin[197], S. Petrushanko[197], S. Polikarpov[197], O. Radchenko[197], M. Savina[197], V. Shalaev[197], S. Shmatov[197], S. Shulha[197], Y. Skovpen[197], K. Slizhevskiy[197], V. Smirnov[197], O. Teryaev[197], I. Tlisova[197], A. Toropin[197], N. Voytishin[197], A. Zarubin[197], I. Zhizhin[197], E. Boos[198], V. Bunichev[198], M. Dubinin[198,ce], L. Dudko[198], V. Kim[198,cm], V. Murzin[198], V. Oreshkin[198], V. Savrin[198], A. Snigirev[198], D. Sosnov[198]

[1] *Yerevan Physics Institute, Yerevan, Armenia*
[2] *Institut für Hochenergiephysik, Vienna, Austria*
[3] *Universiteit Antwerpen, Antwerpen, Belgium*
[4] *Vrije Universiteit Brussel, Brussel, Belgium*
[5] *Université Libre de Bruxelles, Bruxelles, Belgium*
[6] *Ghent University, Ghent, Belgium*
[7] *Université Catholique de Louvain, Louvain-la-Neuve, Belgium*
[8] *Centro Brasileiro de Pesquisas Fisicas, Rio de Janeiro, Brazil*
[9] *Universidade do Estado do Rio de Janeiro, Rio de Janeiro, Brazil*
[10] *Universidade Estadual Paulista, Universidade Federal do ABC, São Paulo, Brazil*
[11] *Institute for Nuclear Research and Nuclear Energy, Bulgarian Academy of Sciences, Sofia, Bulgaria*
[12] *University of Sofia, Sofia, Bulgaria*
[13] *Instituto De Alta Investigación, Universidad de Tarapacá, Casilla 7 D, Arica, Chile*
[14] *Universidad Tecnica Federico Santa Maria, Valparaiso, Chile*
[15] *Beihang University, Beijing, China*
[16] *Department of Physics, Tsinghua University, Beijing, China*
[17] *Institute of High Energy Physics, Beijing, China*
[18] *State Key Laboratory of Nuclear Physics and Technology, Peking University, Beijing, China*
[19] *State Key Laboratory of Nuclear Physics and Technology, Institute of Quantum Matter, South China Normal University, Guangzhou, China*

[20] *Sun Yat-Sen University, Guangzhou, China*
[21] *University of Science and Technology of China, Hefei, China*
[22] *Nanjing Normal University, Nanjing, China*
[23] *Institute of Modern Physics and Key Laboratory of Nuclear Physics and Ion-beam Application (MOE) – Fudan University, Shanghai, China*
[24] *Zhejiang University, Hangzhou, Zhejiang, China*
[25] *Universidad de Los Andes, Bogota, Colombia*
[26] *Universidad de Antioquia, Medellin, Colombia*
[27] *University of Split, Faculty of Electrical Engineering, Mechanical Engineering and Naval Architecture, Split, Croatia*
[28] *University of Split, Faculty of Science, Split, Croatia*
[29] *Institute Rudjer Boskovic, Zagreb, Croatia*
[30] *University of Cyprus, Nicosia, Cyprus*
[31] *Charles University, Prague, Czech Republic*
[32] *Escuela Politecnica Nacional, Quito, Ecuador*
[33] *Universidad San Francisco de Quito, Quito, Ecuador*
[34] *Academy of Scientific Research and Technology of the Arab Republic of Egypt, Egyptian Network of High Energy Physics, Cairo, Egypt*
[35] *Center for High Energy Physics (CHEP-FU), Fayoum University, El-Fayoum, Egypt*
[36] *National Institute of Chemical Physics and Biophysics, Tallinn, Estonia*
[37] *Department of Physics, University of Helsinki, Helsinki, Finland*
[38] *Helsinki Institute of Physics, Helsinki, Finland*
[39] *Lappeenranta-Lahti University of Technology, Lappeenranta, Finland*
[40] *IRFU, CEA, Université Paris-Saclay, Gif-sur-Yvette, France*
[41] *Laboratoire Leprince-Ringuet, CNRS/IN2P3, Ecole Polytechnique, Institut Polytechnique de Paris, Palaiseau, France*
[42] *Université de Strasbourg, CNRS, IPHC UMR 7178, Strasbourg, France*
[43] *Centre de Calcul de l'Institut National de Physique Nucleaire et de Physique des Particules, CNRS/IN2P3, Villeurbanne, France*
[44] *Institut de Physique des 2 Infinis de Lyon (IP2I), Villeurbanne, France*
[45] *Georgian Technical University, Tbilisi, Georgia*
[46] *RWTH Aachen University, I. Physikalisches Institut, Aachen, Germany*
[47] *RWTH Aachen University, III. Physikalisches Institut A, Aachen, Germany*
[48] *RWTH Aachen University, III. Physikalisches Institut B, Aachen, Germany*
[49] *Deutsches Elektronen-Synchrotron, Hamburg, Germany*
[50] *University of Hamburg, Hamburg, Germany*
[51] *Karlsruher Institut fuer Technologie, Karlsruhe, Germany*
[52] *Institute of Nuclear and Particle Physics (INPP), NCSR Demokritos, Aghia Paraskevi, Greece*
[53] *National and Kapodistrian University of Athens, Athens, Greece*
[54] *National Technical University of Athens, Athens, Greece*
[55] *University of Ioánnina, Ioánnina, Greece*
[56] *HUN-REN Wigner Research Centre for Physics, Budapest, Hungary*
[57] *MTA-ELTE Lendület CMS Particle and Nuclear Physics Group, Eötvös Loránd University, Budapest, Hungary*
[58] *Faculty of Informatics, University of Debrecen, Debrecen, Hungary*
[59] *HUN-REN ATOMKI – Institute of Nuclear Research, Debrecen, Hungary*
[60] *Karoly Robert Campus, MATE Institute of Technology, Gyongyos, Hungary*
[61] *Panjab University, Chandigarh, India*
[62] *University of Delhi, Delhi, India*
[63] *Indian Institute of Technology Mandi (IIT-Mandi), Himachal Pradesh, India*
[64] *University of Hyderabad, Hyderabad, India*
[65] *Indian Institute of Technology Kanpur, Kanpur, India*
[66] *Saha Institute of Nuclear Physics, HBNI, Kolkata, India*

JHEP07(2026)119

[67] Indian Institute of Technology Madras, Madras, India
[68] IISER Mohali, India, Mohali, India
[69] Tata Institute of Fundamental Research-A, Mumbai, India
[70] Tata Institute of Fundamental Research-B, Mumbai, India
[71] National Institute of Science Education and Research, An OCC of Homi Bhabha National Institute, Bhubaneswar, Odisha, India
[72] Indian Institute of Science Education and Research (IISER), Pune, India
[73] Indian Institute of Technology Hyderabad, Telangana, India
[74] Isfahan University of Technology, Isfahan, Iran
[75] Institute for Research in Fundamental Sciences (IPM), Tehran, Iran
[76] University College Dublin, Dublin, Ireland
[77a] INFN Sezione di Bari, Bari, Italy
[77b] Università di Bari, Bari, Italy
[77c] Politecnico di Bari, Bari, Italy
[78a] INFN Sezione di Bologna, Bologna, Italy
[78b] Università di Bologna, Bologna, Italy
[79a] INFN Sezione di Catania, Catania, Italy
[79b] Università di Catania, Catania, Italy
[80a] INFN Sezione di Firenze, Firenze, Italy
[80b] Università di Firenze, Firenze, Italy
[81] INFN Laboratori Nazionali di Frascati, Frascati, Italy
[82a] INFN Sezione di Genova, Genova, Italy
[82b] Università di Genova, Genova, Italy
[83a] INFN Sezione di Milano-Bicocca, Milano, Italy
[83b] Università di Milano-Bicocca, Milano, Italy
[84a] INFN Sezione di Napoli, Napoli, Italy
[84b] Università di Napoli 'Federico II', Napoli, Italy
[84c] Università della Basilicata, Potenza, Italy
[84d] Scuola Superiore Meridionale (SSM), Napoli, Italy
[85a] INFN Sezione di Padova, Padova, Italy
[85b] Università di Padova, Padova, Italy
[85c] Universita degli Studi di Cagliari, Cagliari, Italy
[86a] INFN Sezione di Pavia, Pavia, Italy
[86b] Università di Pavia, Pavia, Italy
[87a] INFN Sezione di Perugia, Perugia, Italy
[87b] Università di Perugia, Perugia, Italy
[88a] INFN Sezione di Pisa, Pisa, Italy
[88b] Università di Pisa, Pisa, Italy
[88c] Scuola Normale Superiore di Pisa, Pisa, Italy
[88d] Università di Siena, Siena, Italy
[89a] INFN Sezione di Roma, Roma, Italy
[89b] Sapienza Università di Roma, Roma, Italy
[90a] INFN Sezione di Torino, Torino, Italy
[90b] Università di Torino, Torino, Italy
[90c] Università del Piemonte Orientale, Novara, Italy
[91a] INFN Sezione di Trieste, Trieste, Italy
[91b] Università di Trieste, Trieste, Italy
[92] Kyungpook National University, Daegu, Korea
[93] Department of Mathematics and Physics – GWNU, Gangneung, Korea
[94] Chonnam National University, Institute for Universe and Elementary Particles, Kwangju, Korea
[95] Hanyang University, Seoul, Korea
[96] Korea University, Seoul, Korea
[97] Kyung Hee University, Department of Physics, Seoul, Korea

JHEP07(2026)119

[98] *Sejong University, Seoul, Korea*
[99] *Seoul National University, Seoul, Korea*
[100] *University of Seoul, Seoul, Korea*
[101] *Yonsei University, Department of Physics, Seoul, Korea*
[102] *Sungkyunkwan University, Suwon, Korea*
[103] *College of Engineering and Technology, American University of the Middle East (AUM), Dasman, Kuwait*
[104] *Kuwait University – College of Science – Department of Physics, Safat, Kuwait*
[105] *Riga Technical University, Riga, Latvia*
[106] *University of Latvia (LU), Riga, Latvia*
[107] *Vilnius University, Vilnius, Lithuania*
[108] *National Centre for Particle Physics, Universiti Malaya, Kuala Lumpur, Malaysia*
[109] *Universidad de Sonora (UNISON), Hermosillo, Mexico*
[110] *Centro de Investigacion y de Estudios Avanzados del IPN, Mexico City, Mexico*
[111] *Universidad Iberoamericana, Mexico City, Mexico*
[112] *Benemerita Universidad Autonoma de Puebla, Puebla, Mexico*
[113] *University of Montenegro, Podgorica, Montenegro*
[114] *University of Canterbury, Christchurch, New Zealand*
[115] *National Centre for Physics, Quaid-I-Azam University, Islamabad, Pakistan*
[116] *AGH University of Krakow, Krakow, Poland*
[117] *National Centre for Nuclear Research, Swierk, Poland*
[118] *Institute of Experimental Physics, Faculty of Physics, University of Warsaw, Warsaw, Poland*
[119] *Warsaw University of Technology, Warsaw, Poland*
[120] *Laboratório de Instrumentação e Física Experimental de Partículas, Lisboa, Portugal*
[121] *Faculty of Physics, University of Belgrade, Belgrade, Serbia*
[122] *VINCA Institute of Nuclear Sciences, University of Belgrade, Belgrade, Serbia*
[123] *Centro de Investigaciones Energéticas Medioambientales y Tecnológicas (CIEMAT), Madrid, Spain*
[124] *Universidad Autónoma de Madrid, Madrid, Spain*
[125] *Universidad de Oviedo, Instituto Universitario de Ciencias y Tecnologías Espaciales de Asturias (ICTEA), Oviedo, Spain*
[126] *Instituto de Física de Cantabria (IFCA), CSIC-Universidad de Cantabria, Santander, Spain*
[127] *University of Colombo, Colombo, Sri Lanka*
[128] *University of Ruhuna, Department of Physics, Matara, Sri Lanka*
[129] *CERN, European Organization for Nuclear Research, Geneva, Switzerland*
[130] *PSI Center for Neutron and Muon Sciences, Villigen, Switzerland*
[131] *ETH Zurich – Institute for Particle Physics and Astrophysics (IPA), Zurich, Switzerland*
[132] *Universität Zürich, Zurich, Switzerland*
[133] *National Central University, Chung-Li, Taiwan*
[134] *National Taiwan University (NTU), Taipei, Taiwan*
[135] *High Energy Physics Research Unit, Department of Physics, Faculty of Science, Chulalongkorn University, Bangkok, Thailand*
[136] *Tunis El Manar University, Tunis, Tunisia*
[137] *Çukurova University, Physics Department, Science and Art Faculty, Adana, Turkey*
[138] *Hacettepe University, Ankara, Turkey*
[139] *Middle East Technical University, Physics Department, Ankara, Turkey*
[140] *Bogazici University, Istanbul, Turkey*
[141] *Istanbul Technical University, Istanbul, Turkey*
[142] *Istanbul University, Istanbul, Turkey*
[143] *Yildiz Technical University, Istanbul, Turkey*
[144] *Institute for Scintillation Materials of National Academy of Science of Ukraine, Kharkiv, Ukraine*
[145] *National Science Centre, Kharkiv Institute of Physics and Technology, Kharkiv, Ukraine*
[146] *University of Bristol, Bristol, U.K.*
[147] *Rutherford Appleton Laboratory, Didcot, U.K.*
[148] *Imperial College, London, U.K.*

JHEP07(2026)119

[149] *Brunel University, Uxbridge, U.K.*
[150] *Baylor University, Waco, Texas, U.S.A.*
[151] *Bethel University, St. Paul, Minnesota, U.S.A.*
[152] *Catholic University of America, Washington, DC, U.S.A.*
[153] *The University of Alabama, Tuscaloosa, Alabama, U.S.A.*
[154] *Boston University, Boston, Massachusetts, U.S.A.*
[155] *Brown University, Providence, Rhode Island, U.S.A.*
[156] *University of California, Davis, Davis, California, U.S.A.*
[157] *University of California, Los Angeles, California, U.S.A.*
[158] *University of California, Riverside, Riverside, California, U.S.A.*
[159] *University of California, San Diego, La Jolla, California, U.S.A.*
[160] *University of California, Santa Barbara – Department of Physics, Santa Barbara, California, U.S.A.*
[161] *California Institute of Technology, Pasadena, California, U.S.A.*
[162] *Carnegie Mellon University, Pittsburgh, Pennsylvania, U.S.A.*
[163] *University of Colorado Boulder, Boulder, Colorado, U.S.A.*
[164] *Cornell University, Ithaca, New York, U.S.A.*
[165] *Fermi National Accelerator Laboratory, Batavia, Illinois, U.S.A.*
[166] *University of Florida, Gainesville, Florida, U.S.A.*
[167] *Florida State University, Tallahassee, Florida, U.S.A.*
[168] *Florida Institute of Technology, Melbourne, Florida, U.S.A.*
[169] *University of Illinois Chicago, Chicago, Illinois, U.S.A.*
[170] *The University of Iowa, Iowa City, Iowa, U.S.A.*
[171] *Johns Hopkins University, Baltimore, Maryland, U.S.A.*
[172] *The University of Kansas, Lawrence, Kansas, U.S.A.*
[173] *Kansas State University, Manhattan, Kansas, U.S.A.*
[174] *University of Maryland, College Park, Maryland, U.S.A.*
[175] *Massachusetts Institute of Technology, Cambridge, Massachusetts, U.S.A.*
[176] *University of Minnesota, Minneapolis, Minnesota, U.S.A.*
[177] *University of Nebraska-Lincoln, Lincoln, Nebraska, U.S.A.*
[178] *State University of New York at Buffalo, Buffalo, New York, U.S.A.*
[179] *Northeastern University, Boston, Massachusetts, U.S.A.*
[180] *Northwestern University, Evanston, Illinois, U.S.A.*
[181] *University of Notre Dame, Notre Dame, Indiana, U.S.A.*
[182] *The Ohio State University, Columbus, Ohio, U.S.A.*
[183] *Princeton University, Princeton, New Jersey, U.S.A.*
[184] *University of Puerto Rico, Mayaguez, Puerto Rico, U.S.A.*
[185] *Purdue University, West Lafayette, Indiana, U.S.A.*
[186] *Purdue University Northwest, Hammond, Indiana, U.S.A.*
[187] *Rice University, Houston, Texas, U.S.A.*
[188] *University of Rochester, Rochester, New York, U.S.A.*
[189] *Rutgers, The State University of New Jersey, Piscataway, New Jersey, U.S.A.*
[190] *University of Tennessee, Knoxville, Tennessee, U.S.A.*
[191] *Texas A&M University, College Station, Texas, U.S.A.*
[192] *Texas Tech University, Lubbock, Texas, U.S.A.*
[193] *Vanderbilt University, Nashville, Tennessee, U.S.A.*
[194] *University of Virginia, Charlottesville, Virginia, U.S.A.*
[195] *Wayne State University, Detroit, Michigan, U.S.A.*
[196] *University of Wisconsin – Madison, Madison, Wisconsin, U.S.A.*
[197] *An institute or international laboratory covered by a cooperation agreement with CERN*
[198] *An institute formerly covered by a cooperation agreement with CERN*

[a] *Also at Yerevan State University, Yerevan, Armenia*
[b] *Also at TU Wien, Vienna, Austria*

[c] Also at Ghent University, Ghent, Belgium
[d] Also at FACAMP – Faculdades de Campinas, Sao Paulo, Brazil
[e] Also at Universidade do Estado do Rio de Janeiro, Rio de Janeiro, Brazil
[f] Also at Universidade Estadual de Campinas, Campinas, Brazil
[g] Also at Federal University of Rio Grande do Sul, Porto Alegre, Brazil
[h] Also at The University of the State of Amazonas, Manaus, Brazil
[i] Also at University of Chinese Academy of Sciences, Beijing, China
[j] Also at China Center of Advanced Science and Technology, Beijing, China
[k] Also at University of Chinese Academy of Sciences, Beijing, China
[l] Also at School of Physics, Zhengzhou University, Zhengzhou, China
[m] Now at Henan Normal University, Xinxiang, China
[n] Also at University of Shanghai for Science and Technology, Shanghai, China
[o] Now at The University of Iowa, Iowa City, Iowa, U.S.A.
[p] Also at Center for High Energy Physics, Peking University, Beijing, China
[q] Also at Zewail City of Science and Technology, Zewail, Egypt
[r] Also at British University in Egypt, Cairo, Egypt
[s] Now at Ain Shams University, Cairo, Egypt
[t] Also at Purdue University, West Lafayette, Indiana, U.S.A.
[u] Also at Université de Haute Alsace, Mulhouse, France
[v] Also at Another institute or international laboratory covered by a cooperation agreement with CERN
[w] Also at University of Hamburg, Hamburg, Germany
[x] Also at RWTH Aachen University, III. Physikalisches Institut A, Aachen, Germany
[y] Also at Bergische University Wuppertal (BUW), Wuppertal, Germany
[z] Also at Brandenburg University of Technology, Cottbus, Germany
[aa] Also at Forschungszentrum Jülich, Juelich, Germany
[ab] Now at RWTH Aachen University, III. Physikalisches Institut A, Aachen, Germany
[ac] Also at CERN, European Organization for Nuclear Research, Geneva, Switzerland
[ad] Also at HUN-REN ATOMKI – Institute of Nuclear Research, Debrecen, Hungary
[ae] Now at Universitatea Babes-Bolyai – Facultatea de Fizica, Cluj-Napoca, Romania
[af] Also at MTA-ELTE Lendület CMS Particle and Nuclear Physics Group, Eötvös Loránd University, Budapest, Hungary
[ag] Also at HUN-REN Wigner Research Centre for Physics, Budapest, Hungary
[ah] Also at Physics Department, Faculty of Science, Assiut University, Assiut, Egypt
[ai] Also at The University of Kansas, Lawrence, Kansas, U.S.A.
[aj] Also at Punjab Agricultural University, Ludhiana, India
[ak] Also at University of Hyderabad, Hyderabad, India
[al] Also at Indian Institute of Science (IISc), Bangalore, India
[am] Also at University of Visva-Bharati, Santiniketan, India
[an] Also at IIT Bhubaneswar, Bhubaneswar, India
[ao] Also at Institute of Physics, Bhubaneswar, India
[ap] Also at Deutsches Elektronen-Synchrotron, Hamburg, Germany
[aq] Also at Isfahan University of Technology, Isfahan, Iran
[ar] Also at Sharif University of Technology, Tehran, Iran
[as] Also at Department of Physics, University of Science and Technology of Mazandaran, Behshahr, Iran
[at] Also at Department of Physics, Faculty of Science, Arak University, ARAK, Iran
[au] Also at Helwan University, Cairo, Egypt
[av] Also at Italian National Agency for New Technologies, Energy and Sustainable Economic Development, Bologna, Italy
[aw] Also at Centro Siciliano di Fisica Nucleare e di Struttura Della Materia, Catania, Italy
[ax] Also at Università degli Studi Guglielmo Marconi, Roma, Italy
[ay] Also at Scuola Superiore Meridionale, Università di Napoli 'Federico II', Napoli, Italy
[az] Also at Fermi National Accelerator Laboratory, Batavia, Illinois, U.S.A.
[ba] Also at Lulea University of Technology, Lulea, Sweden

[bb] Also at Consiglio Nazionale delle Ricerche – Istituto Officina dei Materiali, Perugia, Italy
[bc] Also at UPES – University of Petroleum and Energy Studies, Dehradun, India
[bd] Also at Institut de Physique des 2 Infinis de Lyon (IP2I), Villeurbanne, France
[be] Also at Department of Applied Physics, Faculty of Science and Technology, Universiti Kebangsaan Malaysia, Bangi, Malaysia
[bf] Also at Trincomalee Campus, Eastern University, Sri Lanka, Nilaveli, Sri Lanka
[bg] Also at Saegis Campus, Nugegoda, Sri Lanka
[bh] Also at National and Kapodistrian University of Athens, Athens, Greece
[bi] Also at Ecole Polytechnique Fédérale Lausanne, Lausanne, Switzerland
[bj] Also at Universität Zürich, Zurich, Switzerland
[bk] Also at Stefan Meyer Institute for Subatomic Physics, Vienna, Austria
[bl] Also at Near East University, Research Center of Experimental Health Science, Mersin, Turkey
[bm] Also at Konya Technical University, Konya, Turkey
[bn] Also at Izmir Bakircay University, Izmir, Turkey
[bo] Also at Adiyaman University, Adiyaman, Turkey
[bp] Also at Bozok Universitetesi Rektörlügü, Yozgat, Turkey
[bq] Also at Istanbul Sabahattin Zaim University, Istanbul, Turkey
[br] Also at Marmara University, Istanbul, Turkey
[bs] Also at Milli Savunma University, Istanbul, Turkey
[bt] Also at Informatics and Information Security Research Center, Gebze/Kocaeli, Turkey
[bu] Also at Kafkas University, Kars, Turkey
[bv] Now at Istanbul Okan University, Istanbul, Turkey
[bw] Also at Istanbul University – Cerrahpasa, Faculty of Engineering, Istanbul, Turkey
[bx] Also at Istinye University, Istanbul, Turkey
[by] Also at Yildiz Technical University, Istanbul, Turkey
[bz] Also at School of Physics and Astronomy, University of Southampton, Southampton, U.K.
[ca] Also at Monash University, Faculty of Science, Clayton, Australia
[cb] Also at Università di Torino, Torino, Italy
[cc] Also at Karamanoğlu Mehmetbey University, Karaman, Turkey
[cd] Also at California Lutheran University;, Thousand Oaks, California, U.S.A.
[ce] Also at California Institute of Technology, Pasadena, California, U.S.A.
[cf] Also at United States Naval Academy, Annapolis, Maryland, U.S.A.
[cg] Also at Bingol University, Bingol, Turkey
[ch] Also at Georgian Technical University, Tbilisi, Georgia
[ci] Also at Sinop University, Sinop, Turkey
[cj] Also at Erciyes University, Kayseri, Turkey
[ck] Also at Horia Hulubei National Institute of Physics and Nuclear Engineering (IFIN-HH), Bucharest, Romania
[cl] Now at Another institute formerly covered by a cooperation agreement with CERN
[cm] Also at Another institute formerly covered by a cooperation agreement with CERN
[cn] Also at Hamad Bin Khalifa University (HBKU), Doha, Qatar
[co] Also at Yerevan Physics Institute, Yerevan, Armenia
[cp] Also at Imperial College, London, U.K.
[cq] Now at Yerevan Physics Institute, Yerevan, Armenia
[†] Deceased

JHEP07(2026)119